Petri Net computational modelling of Langerhans cell Interferon Regulatory Factor Network predicts their role in T cell activation.

Authors: Marta E. Polak, MSc, PhD*[1,2], Chuin Ying Ung[1], MD, Joanna Masapust[1], MSc, Tom C. Freeman, PhD[3,4] , Michael R. Ardern-Jones, BSc, FRCP, DPhil[1,4]

[1] Clinical and Experimental Sciences, Sir Henry Wellcome Laboratories, Faculty of Medicine, University of Southampton, SO16 6YD, Southampton, UK

[2] Institute for Life Sciences, University of Southampton, SO17 1BJ, UK.

[3] The Roslin Institute and Royal (Dick) School of Veterinary Studies, University of Edinburgh, Easter Bush, Edinburgh, Midlothian EH25 9RG, UK

[4] These authors contributed equally to this work

***Corresponding Author:**

Dr. Marta E. Polak,

Address: Clinical and Experimental Sciences, Faculty of Medicine, University of Southampton, Southampton General Hospital, LE59, MP813, SO16 6YD, Southampton, UK

Tel: 02381205727, e-mail: m.e.polak@soton.ac.uk

Abstract:

Langerhans cells (LCs) are able to orchestrate adaptive immune responses in the skin by interpreting the microenvironmental context in which they encounter foreign substances, but the regulatory basis for this has not been established. Utilising systems immunology approaches combining *in silico* modelling of a reconstructed gene regulatory network (GRN) with *in vitro* validation of the predictions, we sought to determine the mechanisms of regulation of immune responses in human primary LCs. The key role of Interferon regulatory factors (IRFs) as controllers of the human Langerhans cell response to epidermal cytokines was revealed by whole transcriptome analysis. Applying Boolean logic we assembled a Petri net-based model of the IRF-GRN which provides molecular pathway predictions for the induction of different transcriptional programmes in LCs. *In silico* simulations performed after model parameterisation with transcription factor expression values predicted that human LC activation of antigen-specific CD8 T cells would be differentially regulated by epidermal cytokine induction of specific IRF-controlled pathways. This was confirmed by *in vitro* measurement of IFN-g production by activated T cells. As a proof of concept, this approach shows that stochastic modelling of a specific immune networks renders transcriptome data valuable for the prediction of functional outcomes of immune responses.

Introduction

In order for the immune system to provide effective defence against pathogens and xenobiotics, it is critically important that it discriminates between signals that indicate danger and those which are non-threatening and to which a "passive" or "tolerant" response is appropriate. Modulation of immune regulation is of particular importance at body surfaces such as skin, where programming the adaptive immune responses takes place[1]. Here a CD1a high, CD207+ subset of cutaneous dendritic cells, Langerhans' cells (LCs), initiate a rapid immune response to an inflammatory signal from the tissue environment [2,3]. However, in steady state conditions, LCs selectively induce the activation and proliferation of skin-resident regulatory T cells [4,5] that help prevent unwanted immune-mediated reactions.

This important balance is impaired in inflammatory skin conditions such as atopic dermatitis (AD), where disseminated herpes simplex virus (HSV) infection can be life-threatening without effective treatment[6]. Recently a number of risk factors which may predispose patients with AD to develop eczema herpeticum have been identified, including filaggrin mutations, high serum IgE levels and reduced levels of IFN type I and II[7-9]. However, the molecular mechanism underpinning the susceptibility to herpes virus infection remains poorly understood. Aberrations observed in eczema herpeticum patients point to the importance of impaired anti-viral immune response[10], diminished activation of CD8+ cytotoxic T cells[11], and production of indoleamine 2,3-dioxygenase by antigen presenting cells residing in the skin[12]. We and others have shown, that LCs play a central role in the regulation of CD8 T cell-mediated cytotoxic immunity through their unique ability to efficiently cross-present antigens and induce effective CD8 T cell responses [2,3,13]. In atopic disease the ability of skin dendritic cells to polarise adaptive immune responses towards Th2 and Th22 through the effect of aberrant cytokine signalling has been documented in previous studies[1,14-16]. However, little is known of how this signalling affects the ability of LCs to induce CD8 T cell function.

A growing body of evidence suggests that the decision processes which control immune activation or tolerance are executed via simultaneous signalling through multiple transcription factors interconnected in complex molecular networks[17,18]. In particular, immune regulation at the transcriptomic level seems to be executed via gene regulatory networks (GRN). These provide causal molecular explanations for cellular behaviour and execution of transcriptomic programmes, as they detail in a directed manner the flow of genomic information and the control of cellular outputs[19,22,23].

The ability to comprehensively analyse signalling events in LC GRN is essential for understanding of immune regulation in human skin. While it is relatively easy to manipulate the stimulus properties and environmental conditions *in vitro*, the comprehensive assessment of the signalling dynamics in intact human skin is beyond the limits of experimental science. Computational modelling offers the most promising way to approach the problem, providing the mathematical framework for modelling the resting state of signalling systems, including disease-specific steady states, predicting the cell and system behaviour during prolonged exposure to signalling stimulus, and the outcome of multiple signalling events. [19,20].

Quantitative models, using Michaelis-Menten kinetics-based rate laws [21] and mass action kinetic models [22], have been successfully used for simulating small biological networks. They have provided insights into the mechanisms regulating gene, signalling and metabolic regulatory network behaviour. However, the inherent limitation of such an approach lies with the requirement for input of detailed kinetic parameters and relationships within the network, hence constraining the models to relatively small sized networks. For analysis and modelling of large molecular networks, including metabolic networks [23], signalling networks [24] and gene regulatory networks [25], Petri nets have recently emerged as a promising tool. The approach allows the user to vary inputs, which then create a signal flow through the network based solely on the network connectivity, eliminating the necessity for multiple kinetic parameters at each step. The network model was first validated to recapitulate outcomes reported in the literature, including dendritic cells and macrophage subsets[26-35].

Subsequently they have been used to model experimental data derived from whole transcriptome analysis of human Langerhans cells.

To understand better the molecular cross-talk between the structural cells and LC orchestrating adaptive immune responses, we have applied a bioinformatic analysis of transcriptomics data. This allows network inference and dynamic simulation of the behaviour of transcription factor networks and experimental validation of model predictions. Combining bioinformatics analysis with *in vitro* experiments has allowed us to characterise the differential effect of key epidermal cytokines, TNFα and TSLP, on the ability of LCs to cross-present viral antigens to cytotoxic T cells, and to propose a transcriptional mechanism regulating this process.

Results

1) Epidermal cytokines, TNFα and TSLP, differentially regulate the expression of Interferon Regulatory Factors in human migratory LCs.

Our recent study documented that TNFα-matured LCs express a characteristic molecular signature comprising genes involved in antigen capture, intracellular trafficking and formation of immunoproteasome, rendering them superior activators of anti-viral CD8 T cell responses[2]. To analyse how this molecular signature is regulated by signalling from atopic keratinocytes, we measured the whole transcriptome expression of the human migratory LCs (85%-96% CD1a+/HLA-DR+ (Figure 1 a)) during a time course stimulation with TSLP. Bayesian Estimation of Temporal Regulation (BETR) [36] identified 870 probesets up-regulated at 2 h, 349 up-regulated at 8 h and 280 up-regulated at 24 h of stimulation with TSLP in comparison to unstimulated migratory cells. Following exposure to TNFα, probesets up-regulated were 789, 524, and 482 at the corresponding time points. TSLP induced down-regulation of 118 probesets (2 h), 618 probesets (8 h) and 613 probesets (24 h) (compared to 302, 895, and 772 probesets down-regulated by TNFα at the corresponding time points, 1 fold difference in log2(x) robust multichip average (RMA)-normalized expression level between the time point and control, BETR $p<0.05$). Comparative analysis of whole transcriptome data from human LCs matured with TNFα or TSLP defined a core signature of 527 genes as being differentially regulated (maSigPro algorithm [37], $p<0.05$) by the two cytokines (Figure 1b). A transcript-to-transcript Pearson correlation matrix was calculated, a graph constructed in BioLayout *Express*[3D38] ($r = \geq 0.8$) and subjected to clustering using Markov Clustering Algorithm (MCL)[39] with an inflation value set at 1.7 (this controls the granularity of clustering) and the smallest cluster size set at 5. The analysis identified 18 clusters, 5 preferentially up-regulated by TNFα. The two largest clusters (01 and 02) of genes are involved in induction of immune responses and underpinning the cellular processing of antigens (Figure 1b). They included genes encoding proteins involved in antigen capture (*CAV1*), intracellular trafficking (*SNX10* and *SNX11*) and formation of immunoproteasome (*PSME2, PSME3, PSMB10*), (Figure 1c). The 13

smaller clusters induced preferentially by TSLP included genes involved in kinase signalling, peroxisome function and nucleotide metabolism. The full details of gene ontology enrichment of the identified clusters are listed in Table 1, p values calculated using 2way repeated measurement paired ANOVA, for time and cytokine variable.

Table 1. Gene Ontology enrichment in clusters preferentially induced by TNFα or TSLP signalling.

Cluster	Preferentially regulated by (time, cytokine, two way ANOVA)	gene number	GO (FDR B&H) / gene list for low gene number clusters
01	TNFα ($p<0.0001$, $p = 0.021$)	95	immune response ($p = 0.0051$), leukocyte activation ($p = 0.0051$), proteasome activator complex ($p = 0.009$)
02	TNFα ($p<0.0001$, $p = 0.011$)	84	Pathways: cell cycle ($p = 0.008$), HIV infection ($p = 0.012$), proteasome ($p = 0.036$), cross-presentation of soluble exogenous antigens (endosomes) ($p = 0.036$),
09	TNFα ($p<0.0001$, $p = 0.052$)	12	regulation of RNA splicing ($p =0.015$)
17	TNFα ($p<0.0001$, $p = 0.018$)	6	*CLIP2, IL1R2, OAF, RAB38, TCF7, TMEM184C*
18	TNFα ($p=0.0002$, $p = 0.002$)	6	*C17orf62, C19orf54, CPNE1, FTSJD2, HECW1, STK25*
03	TSLP ($p<0.0001$, $p = 0.005$)	36	no annotation
04	TSLP ($p = 0.006$, $p = 0.001$)	25	no annotation
05	TSLP ($p<0.0001$, $p = 0.019$)	25	JUN kinase binding ($p = 0.027$)
06	TSLP ($p<0.0001$, $p = 0.001$)	18	peroxisome proliferator activated receptor binding ($p = 0.017$)
07	TSLP ($p<0.0001$, $p = 0.004$)	18	no annotation
08	TSLP ($p<0.0001$, $p = 0.007$)	16	nucleotide transferase activity ($p = 0.026$)

10	TSLP (p<0.0001, p = ns)	10	nucleotide metabolism (p = 0.042)
11	TSLP (p<0.0001, p = 0.022)	10	mRNA splicing (p = 0.025)
12	TSLP (p=0.0007, p = 0.021)	10	Golgi aparatus (p = 0.025)
13	TSLP (p<0.0001, p = 0.038)	9	transferrin receptor activity ((p = 0.001)
14	TSLP (p= 0.0014, p = 0.003)	8	*ATP5L, EFHA1, ID2, INIP, RECQL, RPS4X, TMSB4X, UBL5*
15	TSLP (p<0.0001, p = 0.054)	8	*CAMK1D, ELL3, LAP3, MLLT4, MPC1, NET1, NFE2L3, STOM*
16	TSLP (p<0.0001, p = ns)	7	*ARAP1, CNDP2, GSDMD, N4BP2L2, NINJ2, PARP10, VPS13B*

To better understand the gene regulatory networks we analysed the expression modules of co-expressed LC genes, and the identified promoter motifs and corresponding transcription factors (TF) which regulate their expression. In LCs treated with the two cytokines the differentially regulated genes contained a possible IRF binding site STTTCRNTTT as the main binding site enriched in the gene signature (ToppGene [40], BH p=0.0125). Analysis of the expression of transcription factors indicated that at T_0 *ZFP36L1*, *NFKBIA*, and *NFKB1* were the most highly expressed transcription factors. However, following stimulation of LC with the inflammatory cytokine TNFα, there was dramatic up-regulation of *IRF1* and *IRF8* transcripts (6.7 and 13.5 fold respectively) at the earliest time point, BETR, p<0.001) (Figure 1d). In agreement with their potential role as mediators of LC responses to TNFα and TSLP, the top differentially regulated TFs were *IRF1*, *IRF4* and *IRF8*, and IRF transcriptional partners including *JUN, ATF3, BATF, BATF3;* (assessed both from absolute expression levels and fold change difference (Figure 1d and Supplementary Figure S1)). The dependence of *IRF1* and *IRF4* expression levels on the cytokines present in the tissue microenvironment was further confirmed in LCs migrating from the epidermal biopsies exposed to TNFα or TSLP (Figure 1e).

2) Stochastic simulation of a logic-based diagram of the IRF gene regulatory network with Petri Nets allows recapitulation of dendritic cell- induced T cell polarisation.

To regulate the cellular functional outcome, IRFs interact in a synergistic or antagonistic manner with other transcription factors and adaptor molecules[41-44]. We hypothesised that these interactions create a gene regulatory network encoding the transcriptional programmes in dendritic cells. To address the complexity of the interactions within this GRN, we assembled a logic-based diagram to capture the multiple reported interactions between IRFs, IRF transcription partners and DNA sequences, orchestrating gene transcription, cell function, and thus, the outcome of immune stimulation[45 46] (Supplementary Materials and Methods, Table S1-S4, Supplementary Figure S2). To identify components for the IRF-GRN, a systematic search was performed in PubMed for terms describing involvement of IRFs in dendritic cell function, antigen presentation and T cell function (Supplementary Table S1). From the 618 returned papers, 83 unique original papers were identified, describing regulation of gene expression by IRF and their transcription partners (Table S2). The data has been structured into an interaction database containing entries for: 1) and 2) interaction partners, 3) mode of interaction, 4) DNA sequence, 5) regulated genes, 6) biological process. This was subsequently converted into a matrix of Boolean interactions between the network components (table S3) and computationally modelled using a version of Stochastic Petri Nets (SPN)[46]. For a detailed description of a diagram assembly please refer to Livigni et al, 2016 and the methods section of this manuscript.[45]

The initial validation of the IRF-GRN was performed using theoretical quantities, where "0" represented lack of transcription factor expression, corresponding to a gene knock/out model. *In silico* simulation using the SPN algorithm (initial marking set up as a theoretical value either 0 (null expression) or 100 (expressed gene) for all possible combinations of the entry nodes: IRF1, IRF4, IRF8, AP1-binding and ETS-binding) demonstrated that the model correctly re-capitulates the observations from multiple experimental systems (Table S2, Figure 2, Figure S2). The data describe

the involvement of IRFs and their transcriptional partners in regulation of a "stereotypical" antigen presenting cell function of a dendritic cell/macrophage lineage. As shown in Figure 2b, all the conditions outlined have been met by the *in silico* model of the GRN. As reported by others, induction of Th1 responses required expression of either IRF1 alone or a combination of IRF8 and ETS transcriptional partners [26-28,33] (Figure 2a, Table S2), while expression of Th2/Th17 was critically dependent on simultaneous expression of IRF4:ETS[29-31] (Th2, Figure 2b, Table S2) or IRF4:AP-1[32,47] (Th17 Figure 2d, Table S2) binding partners. Likewise, the simulation recapitulated a cooperative involvement of IRFs and their transcription partners for induction of antigen presentation by MHC class I molecules, resulting in activation of CD8 T lymphocytes (in agreement with data from existing literature, Table S2, S3)[33,34,42]. It predicted that optimal induction of CD8 T cell activation requires signalling via both IRF1 and IRF8 (Figure 2c)[35].

3) The modulation by epidermal cytokines of LC ability to activate antigen-specific CD8 T cell responses is predicted by *in silico* modelling of IRF-GRN parametrised with experimental data.

One of the more surprising findings emerging from the initial studies of networks and component interactions in different cell types is the multi-functionality ('functional pleiotropism') of signalling networks. This suggests that biological networks have evolved to enable passing of biologically distinct information through shared channels[48]. In essence, while the GRN architecture and main components are shared between different cell types, the spectrum of output genes regulated by the network varies with the specific cell type. This can be illustrated by the fact that although, for Th1-polarising dendritic cells, IRF1-controlled IL12p70 production appears established[26,49], we and others have demonstrated that IL12p70 is not produced by human LCs [2,13,50,51]. This is despite the rapid up-regulation of *IRF1* transcripts in LCs upon stimulation (Figure 1d). The presented IRF-GRN has been assembled by us based on published data derived from multiple cell types. Therefore, to model

199 the IRF-dependent programming within LC we adapted the generic IRF-GRN to represent the
200 interactions reported in human primary LCs.

201 To test the ability of human LC to regulate adaptive immune responses, the GRN model was
202 expanded to include all the members of AP-1 and ETS family found to be expressed in human LCs,
203 determined by microarray analysis [2] (Table S6). Furthermore, the network was enriched in elements
204 representing output genes derived from existing IRF1, IRF4, and IRF8 ChiP-seq data (Table S4) and
205 filtered to include only the genes expressed by human LCs, as measured by microarray experiments
206 (GSE23618, GSE16395, GSE35340, GSE49475, Figure 3). A series of values representing changing
207 levels of LC gene expression (derived from the microarray data) over the time course of stimulation
208 with TNFα or TSLP provided the initial values for all entry nodes (Table S6, Supplementary
209 executable model files: http://www.virtuallyimmune.org/irf-grn/). Stochastic simulation of the flow of
210 tokens through the network and the assessment of token accumulation in the network output nodes
211 provided *in silico* predictions of the pattern of gene expression in LCs during the time course of
212 stimulation by TNF-α and TSLP. It also revealed their potential to induce different immune responses.
213 Analysing the patterns of token accumulation at the network output nodes identified two distinct
214 programmes of gene expression, "A" and "B". Programme "A" included genes preferentially induced
215 by TNFα after binding of transcription factors to ISRE and "B" comprised genes regulated in similar
216 manner by TNFα and TSLP, induced after transcription factor binding to EICE (Figure S3). The results
217 of simulation experiments correctly predicted whether the gene expression profile, as measured
218 experimentally, belonged to programme "A" (genes up-regulated by TNFα) or programme "B" for 34
219 out of 50 of the network output genes. Predictions included genes associated with antigen presentation
220 (*HLA-A*, *-B*, *-C*, *CIITA*, *HLA-DR*), immunoproteasome (*PSME1*, *PSME2*, *PSMB10*), LC activation
221 (*CD40*), and endocytosis (*CAV1*) (Figure 4a-f, Table S5, Supplementary Figure S3). Furthermore,
222 simulation experiments indicated that the ability of LCs to present a peptide to CD8 T cells would be
223 altered by the cytokine milieu (TNFα / TSLP), which has not previously been reported and was not

anticipated. To test the *in silico* predictions, we have examined the ability of LC to cross-present antigens to antigen-specific CD8 T lymphocytes, utilising a long peptide (30 amino acid) containing the EBV BMLF-1 epitope. This epitope is restricted to HLA-A2 and requires intracellular processing for subsequent cross-presentation into the MHC Class I pathway[2,3]. Consistent with the model prediction, maturation by TSLP diminished the capacity of LC to cross-present a viral epitope to antigen-specific CD8 T cells (Figure 4g,h, n=5, $p<0.05$, Figure S4) whereas this was enhanced by TNFα.

Subsequently, to test if the model was capable of predicting LC behaviour when they have been exposed to signals or perturbations within intact epidermis, we targeted signalling of PI3Kγ. This kinase is highly expressed by LC, in contrast to dermal Dendritic Cells (Polak et al 2014)[2] and is one of the most up-regulated genes induced by TSLP (Table 1, Cluster 05). *Ex vivo* epidermal biopsies were cultured in the presence or absence of AS605240, a potent, cell-permeable and ATP-competitive inhibitor of PI3Kγ [52] (Figure S5a). Migratory LC (Figure S5b) were harvested 48h later from inhibitor exposed and non-exposed biopsies and the LC transcriptome assessed using Affymetrix Human Gene ST 1.1 microarrays (n=2 independent donors).

The *in silico* simulations, run using normalised transcription levels as the initial marking for IRF-GRN input nodes (Table S7), predicted that the ability of LC to induce activation of Th1 but not Th2 responses will be diminished by the inhibitor (Figure S5c,d). To validate the *in silico* predictions and assess the ability of LC to prime and polarise adaptive immune responses, LC were co-cultured with allogeneic naïve CD4 T cells for 6 days. Secretion of IFNγ and IL-4 by primed T cells was used as a proxy for Th1 and Th2 polarisation (Figure S5e,f, n=6, in triplicate, mean± SEM shown). As shown in Figure S5, *in vitro* validation confirmed that the PI3Kγ inhibitor reduced the LCs ability to induce Th1 immune responses ($p<0.05$) The observed trend in reducing production IL-4 was not statistically significant, as predicted *in silico*.

Discussion

Molecular targeting of key signals in the immune system has already demonstrated significant advances in the treatment of human disease including cancer and inflammation. These new therapies depend on targeting single molecules or pathways. To date, most such treatments have focused on known effector pathways in immunity such as T cell cytokines. However, yet undiscovered potential lies in targeting factors critical to maintenance of the aberrant immune responses, for which dendritic cells are likely to hold the key. Here, we proposed to investigate in detail the role of immune regulation at the level of transcriptomic networks in human LCs responding to cytokine signals, modelling inflamed epidermis. LCs' anatomical location in the outermost part of the skin and mucosal tissue, combined with their classical capacity for antigen capture, processing and presentation, make a strong case for their role as the primary gatekeepers against infection and other exogenous pro-inflammatory stimuli. By focusing on a key control element of immune regulation by LCs, we have identified the molecular basis for the orchestration of epidermal immunity, which may potentially offer molecular targets for immune intervention.

Analysis of transcriptional networks allowed us to identify a set of transcription factors from the Interferon Regulatory Factors (IRF) family, as a key GRN operating in human LCs. IRFs are critical regulatory molecules for dendritic cell development and function [42,53,54], as well as for efficient regulation of immune responses to infectious pathogens [26,55,56]. The importance of IRFs for tissue homeostasis has been further highlighted by the association of the causal disease variants in GWAS studies. Thus, IRF-binding sequences have been linked with autoimmunity and inflammatory skin disease [57,58], and their key role in driving the Th2 phenotype dominant in asthma and allergic diseases [29]. IRFs function in a network, interacting in a synergistic or antagonistic manner in conjunction with other transcription factors and adaptor molecules, and the subsequent signalling pathway determines functional outcome[41]. Recent years have brought substantial advances in our understanding of GRN and their control of cell differentiation and immune function[29,41,54]. However, there is currently a lack

of evidence to support the application of these advances in the prediction of the outcome of immune stimulation determined by specific tissue disease states.

Dissecting the complexity of a GRN experimentally is challenging. However, computational modelling offers a promising way to approach the problem. It can provide a mathematical framework for modelling the resting state of signalling systems, including disease-specific steady states, predicting the cell and system behavior during prolonged exposure to signalling stimulus, and the outcome of multiple signalling events [22,59]. Computational analysis of high throughput data, resulting in the network inference and dynamical simulation of the behaviour of a transcription factor network, has been shown to provide meaningful insights into the mechanisms of signal integration within a dendritic cell [19,20].

As predictive modelling of regulatory networks can greatly improve data analysis and data – driven hypothesis generation, a broad spectrum of mathematical formalism has been developed, allowing network modelling at different levels of detail. Quantitative continuous methods such as ordinary differential equations (ODEs), model the rate of change of each component in the network and provide detailed quantitative information regarding the networks dynamics[60]. ODEs can be used for modelling small scale GRN [20,21,43,61]. For example, Hoffmann's group demonstrates use of ODE in mass action kinetic model of chosen elements of the NFκB molecular network to achieve comprehensive characterization of the relationship between the resting state and the cellular response to stimulation [20,22,62]. They identified distinct temporal profiles of the activity of the central node kinase IKK or transcription factor NFκB[61] and modelled the temporal control of the specificity of a response[63]. However, ODEs require comprehensive knowledge of kinetic parameters, which are unknown for most networks, and therefore their applicability is limited[64-66]. Furthermore, ODE modelling is computationally expensive, and therefore not suitable for large size networks[67].

In contrast, qualitative logic-based models, such as Boolean networks [68] and Petri nets[25,45,69], do not depend on quantitative data but rather on the structure of the network along with a set of logical

299 constraints. Qualitative regulatory networks can be built from local experimental observations or
300 knowledge-based information (gene-gene or gene-protein interactions) [45,46,70]. The main advantage of
301 qualitative networks is finite numbers of possible states making predictions about the dynamics of
302 biological regulatory systems possible despite the lack of kinetic information. Despite being far less
303 reliant on knowledge of rate constants than ODEs, SPN improve the quantification of Boolean
304 networks, increasing the level of detail and faithfulness to reality, yet still preserving the ability to
305 model large networks with relatively high speed (review: [60]). SPNs parametrised with discrete
306 experimental data allows insights into the trends of molecules' activity-levels in response to an external
307 stimulus [24]. In our work, application of the SPN formalism, utilizing Boolean logic, allowed us to
308 reconstruct the molecular interactions within a key gene regulatory network.

309 As with most models, the model proposed here is reductionist in its nature. The link between a
310 gene's expression and protein function is subject to complex post-transcriptional/translational
311 regulation, which potentially limits the inference of transcriptomics data with respect to functional
312 cellular/tissue outcomes. As a qualitative network our model does not include complex relationships
313 between transcription factors and DNA, merely indicating that the interaction takes place. This reflects
314 the combinatorial nature of this process, where interaction with any expressed transcriptional partner
315 is theoretically possible, and thus stochastically modeled[42,71]. Similarly, the model assumes that the
316 expression levels of the output genes directly translate to the protein concentrations, which underpin
317 the interactions with T lymphocytes and cell effector responses. However reductionist, the latter
318 assumption has been recently justified by the work of Csardi and colleagues, whose noise-robust
319 analyses reveal that mRNA levels explain more than 85% of the variation in steady-state protein levels
320 [72].

321 A reductionist approach was necessary to initiate the modelling and be able to derive a
322 workable diagram of the GRN, when cells are stimulated with two opposing, 'clean' biological signals,
323 rather than being exposed to a complex signalling from whole tissue. This allowed us to correctly

predict a previously unreported outcome of immune stimulation based on the limited input information from a gene expression experiment in primary human LC.

Moreover**,** our approach not only corroborated the hypothesis that gene regulatory networks are universal and can be inferred from analysis of different cell populations, but also allowed correct prediction of an outcome of T lymphocyte stimulation by LCs based on the expression values of relatively few network components. As further validation of the approach, *in silico* modelling yielded correct prediction of perturbation of LCs function when the cells were exposed to a PI3Kγ inhibitor in the context of the intact epidermis. This prediction relied on the assumption that when applied to the whole tissue the PI3Kγ inhibitor interacts directly with LCs. As demonstrated extensively by others, PI3Kγ, in contrast to isoforms α and β, is preferentially expressed in cells of the immune system [73-75] and the systemic effect of PI3Kγ inhibition in animal models is observed solely in immune cells[76]. Importantly, evaluation of dendritic cell function in the PI3Kγ$^{-/-}$ mice demonstrated, that the knock-out mice had a selective defect in the number of skin LCs[77] and showed a defective capacity to mount contact hypersensitivity and delayed-type hypersensitivity reactions[77]. Therefore, even though the epidermis harbours other leukocytes, including tissue-resident T lymphocytes[78], which can similarly be affected by the inhibitor, our experiment corroborated the assumption, and demonstrated, that the effect of PI3Kg inhibition in human epidermis can be mediated by LCs.

The low resolution of logic-based models imposes limitations on their predictive power. Nevertheless the presented work is in line with findings by others [24,46] and confirms that the correct prediction of a network's dynamic behavior can be obtained without need for extensive experimentation and computationally expensive parameter estimation.

The comparative analysis of transcriptomics data from human LCs exposed to the contrasting epidermal signals, TNFα and TSLP, allowed us to determine the transcriptional programmes induced by the two cytokines. It has been becoming increasingly clear that *in vitro* culture can regulate the transcriptome as well as the function of cultured cells [79-81]. The direct comparison of effects of TNFα

and TSLP on cells cultured in otherwise identical conditions allowed us to identify genes differentially regulated by these two cytokines, while the differences induced by the culture conditions were removed by the maSigPro algorithm. The most significant differences were discovered in the genes encoding the ability of LCs to process and present antigens. Maturation of LCs in the presence of TSLP resulted in impaired capacity to activate antigen-specific cytotoxic T cells, compared with TNFα-matured LCs. This suggests a role for TSLP in mediating the impaired CD8 T cell responses which may be of particular relevance for atopic diseases such as asthma and atopic dermatitis which are characterized by pre-disposition to viral infections [6,82-84]. Indeed, we and others have shown that LCs are extremely potent inducers of efficient CD8 T cell activation and anti-viral immunity [2,3,13,85]. Even though recent reports suggest a role of antigen exchange between LCs and subsets of dermal dendritic cells, the importance of LC has been demonstrated in murine and human systems, including their role in mediating anti-HSV immune responses through antigen uptake and processing[86,87]. Furthermore, *in vivo*, HSV infections principally target keratinocytes (through HSV nectin-1 expression)[88], and induce keratinocyte apoptosis in the epidermis. Therefore, in early infections, LCs uptake and processing of HSV antigens from apoptotic keratinocytes is likely to be critical.

The proposed model provides a proof of concept, to demonstrate that computational modelling of a specific immune network can predict functional outcomes of immune responses based on experimentally derived transcription levels of selected key molecular hubs. Applying this reductionist approach allowed us to determine the effect of altered cytokine signalling, as would be found in human epidermis under different conditions, and predict the impact on immune responses using easily available data (i.e. gene expression levels).

In this case a high epidermal concentration of TSLP in the milieu of atopic dermatitis would be expected to impair skin immunity against viral infection through IRF signalling pathways, which may be relevant to eczema herpeticum, and may also provide a further rationale for anti-TSLP therapy, or even targeting of IRF, in susceptible individuals.

The validation of the model has so far been limited to the *in vitro* approach, allowing investigations of the LC:T cell interaction in a controlled system. While allowing ease of manipulation, this system does not reflect complex signaling events and cell interactions *in vivo.* In order to be able to use it for the design and testing of therapeutic perturbations, it would be necessary to characterise the disease-related steady state of LCs, and validate the outcome of stimulation predicted by the model at both local (skin) and systemic level, iteratively developing the model to correctly represent the observed outcomes.

We envisage that the outlined approach can provide a platform for many future studies of human immunity, utilising data from individual transcriptomic analyses to provide predictions of how molecular interventions may alter cellular phenotype based on the actual gene expression patterns in an individual. Such comprehensive analyses ultimately enable inferring the influence of the disease state on the cellular response to stimulation. This in turn can determine the outcome of immune responses in health and in disease, and offers the possibility of predictive *in silico* testing of the effectiveness of therapeutic interventions.

Methods:

LC isolation and culture

Skin specimens and blood samples were acquired from healthy individuals after obtaining informed written consent with approval by the Southampton and South West Hampshire Research Ethics Committee in adherence to Helsinki Guidelines. Primary cutaneous DCs were isolated as described previously (5). Briefly, following dispase (2 U/ml, Gibco, UK) digestion of epidermal sheets, migratory LCs were harvested after 48h culture of epidermal fragments. Low density cells were enriched using density gradient centrifugation (Optiprep 1:4.2, Axis Shield, Norway) and purified with CD1a+ magnetic beads according to manufacturer's protocol (Miltenyi Biotec, UK). Epidermal and dermal DCs were purified with magnetic beads according to manufacturer's protocol (epidermal cells: CD1a+, dermal cells: CD11c+, Milenyi Biotec, UK). Cells were assayed for yield and cell viability, and unstimulated cells (time 0, 250,000/cell type/donor) were harvested immediately. For analysis of changes in gene expression upon activation, LCs were stimulated with TNF-α or TSLP (25 ng/ml, 15 ng/ml respectively, Miltenyi Biotec, UK) for 2, 8 and 24h (250,000 cells/cell type/donor/time point). For analysis of epidermal explant culture, epidermal sheets from 6 mm biopsies were cultured with epidermal cytokines as described above, and the RNA was isolated for qRT-PCR gene expression gene analysis from the LCs were harvested 48h later. For pulsing with a nominal CD8+ T cell epitope, LCs were incubated with 10 μM of a proGLC peptide, containing 9 aminoacid HLA-A2 restricted EBV-derived epitope (FNNFTVSFWLRVPKVSASHLEGLCTLVAML; Peptide Protein Research, UK) for 18h, with TNFα added at 6 h, and washed thoroughly before co-culture with T cells. EBV-peptide-specific T cell line was expanded as described in detail previously [2,3]. For PI3Kγ inhibition human epidermal biopsies (6 mm) were exposed to the effects of AS605240 at the non-toxic dose 0.1 uM or 1 μl DMSO (control diluent). Migratory LC were co-cultured with allogeneic naïve CD4 T cells. Secretion of IFNγ and IL-4 was measured in an ELISpot experiment as per manufacturer protocol,

(Mabtech, Sweeden), after 6 days of priming and re-stimulation with phytohemagglutinin (PHA) (n=6, in triplicate).

Microarray data analysis

RNA was isolated using RNeasy mini kits (Qiagen, UK) as per the manufacturer's protocol. RNA concentration and integrity was determined with an Agilent Bioanalyser. All the samples had a RIN >7.0 and were taken forward for labelling. Gene expression analysis was carried out using the Human Genome U-219 Affymetrix platform (LC stimulation with cytokines) or Human Gene ST 1.1 Affymetrix platform, Affymetrix ATLAS system, for cell migrating post PI3Kγ inhibition. Expression data were normalised using the Robust Multichip Average (RMA) package within the Affymetrix expression console package and annotated. After an initial QC check, the data was taken forward for analysis. To identify genes regulated by exposure of LCs to TNFα and TSLP, a cutoff threshold 0.05 of Bayesian estimation of temporal regulation [36] for genes showing x1 log(2)-fold difference between the gene expression level at a given time point and time 0 control. Probesets differentially regulated by TNFα and TSLP, were identified using MaSigPro algorithm (24) $p<0.05$. Using network analysis tool BioLayout *Express*^{3D}[38], a transcript-to-transcript correlation matrix was calculated for 527 probesets fulfilling the criteria above, where each column of data was derived from a different sample (donor/cell type/condition) and each row of data represents an individual probeset (25). A non-directional network graph of the data was generated for a Pearson correlation coefficient of $r \geq 0.80$. In this context, nodes represent individual probesets (genes/transcripts) and the edges between them Pearson correlation coefficients between individual probesets above the threshold value. The network graph was then clustered into groups of genes sharing similar profiles using the MCL algorithm within the BioLayout *Express*^{3D} tool with an MCL inflation value set to 1.7, as reported previously (26). Gene set enrichment analysis was performed using the ''functional annotation clustering'' tool, (similarity threshold 0.5, multiple linkage threshold 0.5, EASE:1.0 and Benjamini correction) from DAVID (27)

and ToppGene [40] web-based analysis tools and confirmed by detailed direct analysis using Gene Expression Atlas (http://www.ebi.ac.uk/gxa/). All microarray data used for these studies are available in GEO, Accession No.: TNFα and TSLP: GSE49475. PI3Kγ : GSE94247.

Model Assembly

To identify components for the IRF GRN a systematic search in PubMed was performed, as summarised in Table S1. Separate searches have been performed for each combination of terms. From the returned papers, 82 unique original papers were identified, describing regulation of gene expression by IRF and their transcription partners (Table S2). The experimental findings within each listed reference papers have been analysed to identify the stimulus, cell type, biological process controlled by IRF (including lists of genes identified by ChIP-seq analysis), the interaction partner, and the DNA binding sequence. This information has been categorised as the network components: input node, transmission node, output node and mode of interaction.

To facilitate the network assembly, the data has been structured into an interaction database, containing entries for: 1) stimulus, 2) interaction partner A, 3) interaction partner B, 4) mode of interaction, 5) DNA sequence, 6) gene transcription/biological process. This information is shown in Table S2. The interaction database was sorted and analysed to identify experimental findings validated by multiple reports. To be included into the network architecture, the interaction had to be confirmed by two independent reports. If any referenced publication reported only part of the information (e.g. only interaction between IRF and transcription partner, but not the DNA sequence) the lacking information have been inferred from the complementing reports.

To convert the database of interactions into a Boolean network, a checkerboard of interactions between the network elements have been assembled (Table S3), assigning for each interaction gate “and”, where both components are essential, “or”, when one of the components is essential or “inhibition”.

462 The network diagram was constructed using yED (yFiles, Germany) following the mEPN notation[46],
463 allowing computational modelling of concurrent systems. For a detailed description of a diagram
464 assembly please refer to Livigni et al, 2016 [45]. Signalling Petri Nets are an extended application of
465 stochastic Petri nets (SPN) originally described by Ruths *et al.*[24]. This method integrates elements of
466 a Boolean network simulator with the synchronized Petri net model for the network represented using
467 the classic Petri net view of places and transitions. In brief, the signalling Petri Net algorithm models
468 the stochastic 'flow' of variable numbers of tokens through the network, solely determined by the
469 initial input values and the network architecture. The tokens are assigned to the GRN entry transitions,
470 and represent quantities of the biological molecules, in case of the IRF-GRN, the levels of expression
471 of the transcript. The amount of tokens assigned at the entry (the network initial marking set-up) can
472 be either theoretical, representing a binary on/off expression levels, corresponding to a biological
473 knock-out situation, or derived from biological experiment, and representing the quantity of the
474 transcript measured in cells.

475

476 **IRF GRN model parametrization and *in silico* simulations**

477 The network diagram has been drawn in a mEPN notation[24] [46], allowing computational
478 modelling of concurrent systems. When formerly constructed as a bipartite graph, nodes represent
479 biological entities and transitions represent biological interactions. The abundance of a molecule at
480 any given network node can be represented by the placement of tokens. Edges connecting the nodes
481 and transitions determine the direction of the token flow through the diagram, representing the progress
482 of the biological process. The detailed description of network assembly can be found in the
483 supplementary material and methods. To validate the graph reachability and correct prediction of the
484 postulated biological effect in the presence of one or many TF, initial marking (number of tokens in
485 the network entry nodes) has been set up as a theoretical value either 0 or 100 for every possible
486 combination of the entry nodes: *IRF1, IRF4, IRF8,* AP1-binding and ETS-binding. To test the network

behavior in physiological conditions, the initial marking of the SPN has been set as per the levels of expression from microarray data analysis, Table S6. Simulations were executed using BioLayout *Express*^{3D}, 100 time blocks, 500 runs.

Acknowledgments

Funding was provided by the British Skin Foundation. MEP is supported by the Wellcome Trust Sir Henry Dale Fellowship. TCF is supported by supported by Biotechnology and Biological Sciences Research Council Grant BB/J004235 and the development of BioLayout *Express*^{3D} was funded by BBSRC grant RA1344. We are grateful to Dr C. Woelk, Dr. M. Brenn and Prof. Peter Friedmann for critical review of the manuscript. We would like to thank Dr. Derek Wright for hosting the executable model files on www.virtuallyimmune.org. We are grateful to Dr Carolann McGuire and Richard Jewell, Flow Cytometry Unit, Faculty of Medicine, University of Southampton, for assistance with flow cytometry analysis. We would like to thank Prof. Mahesan Niranjan for discussing statistical analysis.

Author Contributions

MEP intellectually conceived the idea, conducted the experiments and simulations, analysed the data and assembled the network diagram. CYU and JM optimised and run PI3Kγ inhibition experiment. TCF supervised transcriptomic data analysis, network assembly and simulations. MRAJ supervised experimental design, data acquisition and analysis. MEP, TCF and MRAJ interpreted the data and wrote the manuscript.

Competing financial interests:

Authors declare no competing financial interests.

References

1 Newell, L. *et al.* Sensitization via Healthy Skin Programs Th2 Responses in Individuals with Atopic Dermatitis. *J Invest Dermatol* **133**, 2372-2380, doi:10.1038/jid.2013.148 (2013).

2 Polak, M. E. *et al.* Distinct molecular signature of human skin langerhans cells denotes critical differences in cutaneous dendritic cell immune regulation. *J Invest Dermatol* **134**, 695-703, doi:10.1038/jid.2013.375 (2014).

3 Polak, M. E. *et al.* CD70-CD27 interaction augments CD8+ T-cell activation by human epidermal Langerhans cells. *J Invest Dermatol* **132**, 1636-1644, doi:10.1038/jid.2012.26 (2012).

4 Seneschal, J., Clark, R. A., Gehad, A., Baecher-Allan, C. M. & Kupper, T. S. Human epidermal Langerhans cells maintain immune homeostasis in skin by activating skin resident regulatory T cells. *Immunity* **36**, 873-884, doi:10.1016/j.immuni.2012.03.018 (2012).

5 van der Aar, A. M. *et al.* Langerhans Cells Favor Skin Flora Tolerance through Limited Presentation of Bacterial Antigens and Induction of Regulatory T Cells. *J Invest Dermatol* **133**, 1240-1249, doi:10.1038/jid.2012.500 (2013).

6 Beck, L. A. *et al.* Phenotype of atopic dermatitis subjects with a history of eczema herpeticum. *J Allergy Clin Immunol* **124**, 260-269, 269 e261-267, doi:10.1016/j.jaci.2009.05.020 (2009).

7 Peng, W. M. *et al.* Risk factors of atopic dermatitis patients for eczema herpeticum. *J Invest Dermatol* **127**, 1261-1263, doi:10.1038/sj.jid.5700657 (2007).

8 Gao, P. S. *et al.* Filaggrin mutations that confer risk of atopic dermatitis confer greater risk for eczema herpeticum. *J Allergy Clin Immunol* **124**, 507-513, 513 e501-507, doi:10.1016/j.jaci.2009.07.034 (2009).

9 Leung, D. Y. *et al.* Human atopic dermatitis complicated by eczema herpeticum is associated with abnormalities in IFN-gamma response. *J Allergy Clin Immunol* **127**, 965-973 e961-965, doi:10.1016/j.jaci.2011.02.010 (2011).

10 Scott, J. E. *et al.* Impaired immune response to vaccinia virus inoculated at the site of cutaneous allergic inflammation. *J Allergy Clin Immunol* **120**, 1382-1388, doi:10.1016/j.jaci.2007.08.004 (2007).

11 Mathias, R. A. *et al.* Atopic dermatitis complicated by eczema herpeticum is associated with HLA B7 and reduced interferon-gamma-producing CD8+ T cells. *Br J Dermatol* **169**, 700-703, doi:10.1111/bjd.12382 (2013).

12 Staudacher, A., Hinz, T., Novak, N., von Bubnoff, D. & Bieber, T. Exaggerated IDO1 expression and activity in Langerhans cells from patients with atopic dermatitis upon viral stimulation: a potential predictive biomarker for high risk of Eczema herpeticum. *Allergy*, doi:10.1111/all.12699 (2015).

13 Banchereau, J. *et al.* The differential production of cytokines by human Langerhans cells and dermal CD14(+) DCs controls CTL priming. *Blood* **119**, 5742-5749, doi:10.1182/blood-2011-08-371245 (2012).

14 Ebner, S. *et al.* Thymic stromal lymphopoietin converts human epidermal Langerhans cells into antigen-presenting cells that induce proallergic T cells. *J Allergy Clin Immunol* **119**, 982-990, doi:10.1016/j.jaci.2007.01.003 (2007).

15 Soumelis, V. *et al.* Human epithelial cells trigger dendritic cell mediated allergic inflammation by producing TSLP. *Nat Immunol* **3**, 673-680, doi:10.1038/ni805 (2002).

16 Fujita, H. *et al.* Lesional dendritic cells in patients with chronic atopic dermatitis and psoriasis exhibit parallel ability to activate T-cell subsets. *J Allergy Clin Immunol* **128**, 574-582 e571-512, doi:10.1016/j.jaci.2011.05.016 (2011).

17 Mabbott, N. A., Baillie, J. K., Brown, H., Freeman, T. C. & Hume, D. A. An expression atlas of human primary cells: inference of gene function from coexpression networks. *BMC Genomics* **14**, 632, doi:10.1186/1471-2164-14-632 (2013).
18 Xue, J. *et al.* Transcriptome-based network analysis reveals a spectrum model of human macrophage activation. *Immunity* **40**, 274-288, doi:10.1016/j.immuni.2014.01.006 (2014).
19 Amit, I. *et al.* Unbiased reconstruction of a mammalian transcriptional network mediating pathogen responses. *Science (New York, N.Y.)* **326**, 257-263, doi:10.1126/science.1179050 (2009).
20 Shih, V. F. *et al.* Control of RelB during dendritic cell activation integrates canonical and noncanonical NF-kappaB pathways. *Nat Immunol* **13**, 1162-1170, doi:10.1038/ni.2446 (2012).
21 Laslo, P., Pongubala, J. M., Lancki, D. W. & Singh, H. Gene regulatory networks directing myeloid and lymphoid cell fates within the immune system. *Semin Immunol* **20**, 228-235, doi:10.1016/j.smim.2008.08.003 (2008).
22 Loriaux, P. M. & Hoffmann, A. A framework for modeling the relationship between cellular steady-state and stimulus-responsiveness. *Methods Cell Biol* **110**, 81-109, doi:10.1016/b978-0-12-388403-9.00004-7 (2012).
23 Tian, Z., Faure, A., Mori, H. & Matsuno, H. Identification of key regulators in glycogen utilization in E. coli based on the simulations from a hybrid functional Petri net model. *BMC Syst Biol* **7 Suppl 6**, S1, doi:10.1186/1752-0509-7-s6-s1 (2013).
24 Ruths, D., Muller, M., Tseng, J. T., Nakhleh, L. & Ram, P. T. The signaling petri net-based simulator: a non-parametric strategy for characterizing the dynamics of cell-specific signaling networks. *PLoS Comput Biol* **4**, e1000005, doi:10.1371/journal.pcbi.1000005 (2008).
25 Steggles, L. J., Banks, R., Shaw, O. & Wipat, A. Qualitatively modelling and analysing genetic regulatory networks: a Petri net approach. *Bioinformatics (Oxford, England)* **23**, 336-343, doi:10.1093/bioinformatics/btl596 (2007).
26 Roy, S. *et al.* Batf2/Irf1 Induces Inflammatory Responses in Classically Activated Macrophages, Lipopolysaccharides, and Mycobacterial Infection. *J Immunol* **194**, 6035-6044, doi:10.4049/jimmunol.1402521 (2015).
27 Marecki, S., Riendeau, C. J., Liang, M. D. & Fenton, M. J. PU.1 and multiple IFN regulatory factor proteins synergize to mediate transcriptional activation of the human IL-1 beta gene. *J Immunol* **166**, 6829-6838 (2001).
28 Liu, J., Guan, X., Tamura, T., Ozato, K. & Ma, X. Synergistic activation of interleukin-12 p35 gene transcription by interferon regulatory factor-1 and interferon consensus sequence-binding protein. *J Biol Chem* **279**, 55609-55617, doi:10.1074/jbc.M406565200 (2004).
29 Williams, J. W. *et al.* Transcription factor IRF4 drives dendritic cells to promote Th2 differentiation. *Nature communications* **4**, 2990, doi:10.1038/ncomms3990 (2013).
30 Ahyi, A. N., Chang, H. C., Dent, A. L., Nutt, S. L. & Kaplan, M. H. IFN regulatory factor 4 regulates the expression of a subset of Th2 cytokines. *J Immunol* **183**, 1598-1606, doi:10.4049/jimmunol.0803302 (2009).
31 Tussiwand, R. *et al.* Klf4 expression in conventional dendritic cells is required for T helper 2 cell responses. *Immunity* **42**, 916-928, doi:10.1016/j.immuni.2015.04.017 (2015).
32 Glasmacher, E. *et al.* A genomic regulatory element that directs assembly and function of immune-specific AP-1-IRF complexes. *Science (New York, N.Y.)* **338**, 975-980, doi:10.1126/science.1228309 (2012).
33 Shi, L., Perin, J. C., Leipzig, J., Zhang, Z. & Sullivan, K. E. Genome-wide analysis of interferon regulatory factor I binding in primary human monocytes. *Gene* **487**, 21-28, doi:10.1016/j.gene.2011.07.004 (2011).

34 Gabriele, L. *et al.* IRF-1 deficiency skews the differentiation of dendritic cells toward plasmacytoid and tolerogenic features. *J Leukoc Biol* **80**, 1500-1511, doi:10.1189/jlb.0406246 (2006).
35 Masumi, A., Tamaoki, S., Wang, I. M., Ozato, K. & Komuro, K. IRF-8/ICSBP and IRF-1 cooperatively stimulate mouse IL-12 promoter activity in macrophages. *FEBS Lett* **531**, 348-353 (2002).
36 Aryee, M. J., Gutierrez-Pabello, J. A., Kramnik, I., Maiti, T. & Quackenbush, J. An improved empirical bayes approach to estimating differential gene expression in microarray time-course data: BETR (Bayesian Estimation of Temporal Regulation). *BMC Bioinformatics* **10**, 409, doi:10.1186/1471-2105-10-409 (2009).
37 Conesa, A., Nueda, M. J., Ferrer, A. & Talon, M. maSigPro: a method to identify significantly differential expression profiles in time-course microarray experiments. *Bioinformatics (Oxford, England)* **22**, 1096-1102, doi:10.1093/bioinformatics/btl056 (2006).
38 Freeman, T. C. *et al.* Construction, visualisation, and clustering of transcription networks from microarray expression data. *PLoS Comput Biol* **3**, 2032-2042, doi:10.1371/journal.pcbi.0030206 (2007).
39 Enright, A. J., Van Dongen S Fau - Ouzounis, C. A. & Ouzounis, C. A. An efficient algorithm for large-scale detection of protein families. doi:D - NLM: PMC101833 EDAT-2002/03/28 10:00 MHDA- 2002/05/04 10:01 CRDT- 2002/03/28 10:00 PST - ppublish.
40 Chen, J., Bardes, E. E., Aronow, B. J. & Jegga, A. G. ToppGene Suite for gene list enrichment analysis and candidate gene prioritization. *Nucleic Acids Res* **37**, W305-311, doi:10.1093/nar/gkp427 (2009).
41 Singh, H., Khan, A. A. & Dinner, A. R. Gene regulatory networks in the immune system. *Trends Immunol* **35**, 211-218, doi:10.1016/j.it.2014.03.006 (2014).
42 Tussiwand, R. *et al.* Compensatory dendritic cell development mediated by BATF-IRF interactions. *Nature* **490**, 502-507, doi:10.1038/nature11531 (2012).
43 Ochiai, K. *et al.* A self-reinforcing regulatory network triggered by limiting IL-7 activates pre-BCR signaling and differentiation. *Nat Immunol* **13**, 300-307, doi:10.1038/ni.2210 (2012).
44 Spooner, C. J., Cheng, J. X., Pujadas, E., Laslo, P. & Singh, H. A recurrent network involving the transcription factors PU.1 and Gfi1 orchestrates innate and adaptive immune cell fates. *Immunity* **31**, 576-586, doi:10.1016/j.immuni.2009.07.011 (2009).
45 Livigni, A. *et al.* Petri Net-Based Graphical and Computational Modelling of Biological Systems. *bioRxiv*, doi:10.1101/047043 (2016).
46 O'Hara, L. *et al.* Modelling the Structure and Dynamics of Biological Pathways. *PLoS Biol* **14**, e1002530, doi:10.1371/journal.pbio.1002530 (2016).
47 Li, P. *et al.* BATF-JUN is critical for IRF4-mediated transcription in T cells. *Nature* **490**, 543-546, doi:10.1038/nature11530 (2012).
48 Behar, M. & Hoffmann, A. Understanding the temporal codes of intra-cellular signals. *Curr Opin Genet Dev* **20**, 684-693, doi:10.1016/j.gde.2010.09.007 (2010).
49 Berghout, J. *et al.* Irf8-regulated genomic responses drive pathological inflammation during cerebral malaria. *PLoS Pathog* **9**, e1003491, doi:10.1371/journal.ppat.1003491 (2013).
50 Munz, C. *et al.* Mature myeloid dendritic cell subsets have distinct roles for activation and viability of circulating human natural killer cells. *Blood* **105**, 266-273, doi:10.1182/blood-2004-06-2492 (2005).
51 Ratzinger, G. *et al.* Mature human Langerhans cells derived from CD34+ hematopoietic progenitors stimulate greater cytolytic T lymphocyte activity in the absence of bioactive IL-12p70, by either single peptide presentation or cross-priming, than do dermal-interstitial or monocyte-derived dendritic cells. *J Immunol* **173**, 2780-2791 (2004).

52 Camps, M. *et al.* Blockade of PI3Kgamma suppresses joint inflammation and damage in mouse models of rheumatoid arthritis. *Nat Med* **11**, 936-943, doi:10.1038/nm1284 (2005).
53 Schlitzer, A. *et al.* IRF4 transcription factor-dependent CD11b+ dendritic cells in human and mouse control mucosal IL-17 cytokine responses. *Immunity* **38**, 970-983, doi:10.1016/j.immuni.2013.04.011 (2013).
54 Vander Lugt, B. *et al.* Transcriptional programming of dendritic cells for enhanced MHC class II antigen presentation. *Nat Immunol*, doi:10.1038/ni.2795 (2013).
55 Gupta, M. *et al.* IRF8 directs stress-induced autophagy in macrophages and promotes clearance of Listeria monocytogenes. *Nature communications* **6**, 6379, doi:10.1038/ncomms7379 (2015).
56 Akbari, M. *et al.* IRF4 in dendritic cells inhibits IL-12 production and controls Th1 immune responses against Leishmania major. *J Immunol* **192**, 2271-2279, doi:10.4049/jimmunol.1301914 (2014).
57 Swindell, W. R. *et al.* Psoriasis drug development and GWAS interpretation through in silico analysis of transcription factor binding sites. *Clin Transl Med* **4**, 13, doi:10.1186/s40169-015-0054-5 (2015).
58 Farh, K. K. *et al.* Genetic and epigenetic fine mapping of causal autoimmune disease variants. *Nature* **518**, 337-343, doi:10.1038/nature13835 (2015).
59 Loriaux, P. M., Tesler, G. & Hoffmann, A. Characterizing the relationship between steady state and response using analytical expressions for the steady states of mass action models. *PLoS Comput Biol* **9**, e1002901, doi:10.1371/journal.pcbi.1002901 (2013).
60 Karlebach, G. & Shamir, R. Modelling and analysis of gene regulatory networks. *Nature reviews. Molecular cell biology* **9**, 770-780, doi:10.1038/nrm2503 (2008).
61 Werner, S. L. *et al.* Encoding NF-kappaB temporal control in response to TNF: distinct roles for the negative regulators IkappaBalpha and A20. *Genes Dev* **22**, 2093-2101, doi:10.1101/gad.1680708 (2008).
62 Shih, V. F. *et al.* Kinetic control of negative feedback regulators of NF-kappaB/RelA determines their pathogen- and cytokine-receptor signaling specificity. *Proc Natl Acad Sci U S A* **106**, 9619-9624, doi:10.1073/pnas.0812367106 (2009).
63 Werner, S. L., Barken, D. & Hoffmann, A. Stimulus specificity of gene expression programs determined by temporal control of IKK activity. *Science (New York, N.Y.)* **309**, 1857-1861, doi:10.1126/science.1113319 (2005).
64 Arisi, I., Cattaneo, A. & Rosato, V. Parameter estimate of signal transduction pathways. *BMC neuroscience* **7 Suppl 1**, S6, doi:10.1186/1471-2202-7-s1-s6 (2006).
65 Bailey, J. E. Complex biology with no parameters. *Nature biotechnology* **19**, 503-504, doi:10.1038/89204 (2001).
66 Papin, J. A., Hunter, T., Palsson, B. O. & Subramaniam, S. Reconstruction of cellular signalling networks and analysis of their properties. *Nature reviews. Molecular cell biology* **6**, 99-111, doi:10.1038/nrm1570 (2005).
67 Li, S., Wang, L., Berman, M., Kong, Y. Y. & Dorf, M. E. Mapping a dynamic innate immunity protein interaction network regulating type I interferon production. *Immunity* **35**, 426-440, doi:10.1016/j.immuni.2011.06.014 (2011).
68 Glass, L. & Kauffman, S. A. The logical analysis of continuous, non-linear biochemical control networks. *Journal of theoretical biology* **39**, 103-129 (1973).
69 Peleg, M., Yeh, I. & Altman, R. B. Modelling biological processes using workflow and Petri Net models. *Bioinformatics (Oxford, England)* **18**, 825-837 (2002).
70 Bourdon, J., Eveillard, D. & Siegel, A. Integrating quantitative knowledge into a qualitative gene regulatory network. *PLoS Comput Biol* **7**, e1002157, doi:10.1371/journal.pcbi.1002157 (2011).

71 Friedlander, T., Prizak, R., Guet, C. C., Barton, N. H. & Tkacik, G. Intrinsic limits to gene regulation by global crosstalk. *Nature communications* **7**, 12307, doi:10.1038/ncomms12307 (2016).
72 Csardi, G., Franks, A., Choi, D. S., Airoldi, E. M. & Drummond, D. A. Accounting for experimental noise reveals that mRNA levels, amplified by post-transcriptional processes, largely determine steady-state protein levels in yeast. *PLoS genetics* **11**, e1005206, doi:10.1371/journal.pgen.1005206 (2015).
73 Hirsch, E. *et al.* Central role for G protein-coupled phosphoinositide 3-kinase gamma in inflammation. *Science (New York, N.Y.)* **287**, 1049-1053 (2000).
74 Rommel, C., Camps, M. & Ji, H. PI3K delta and PI3K gamma: partners in crime in inflammation in rheumatoid arthritis and beyond? *Nature reviews. Immunology* **7**, 191-201, doi:10.1038/nri2036 (2007).
75 Banham-Hall, E., Clatworthy, M. R. & Okkenhaug, K. The Therapeutic Potential for PI3K Inhibitors in Autoimmune Rheumatic Diseases. *The open rheumatology journal* **6**, 245-258, doi:10.2174/1874312901206010245 (2012).
76 Winkler, D. G. *et al.* PI3K-delta and PI3K-gamma inhibition by IPI-145 abrogates immune responses and suppresses activity in autoimmune and inflammatory disease models. *Chemistry & biology* **20**, 1364-1374, doi:10.1016/j.chembiol.2013.09.017 (2013).
77 Del Prete, A. *et al.* Defective dendritic cell migration and activation of adaptive immunity in PI3Kgamma-deficient mice. *The EMBO journal* **23**, 3505-3515, doi:10.1038/sj.emboj.7600361 (2004).
78 Clark, R. A. *et al.* Skin effector memory T cells do not recirculate and provide immune protection in alemtuzumab-treated CTCL patients. *Sci Transl Med* **4**, 117ra117, doi:10.1126/scitranslmed.3003008 (2012).
79 Fauque, P. *et al.* In vitro fertilization and embryo culture strongly impact the placental transcriptome in the mouse model. *PLoS One* **5**, e9218, doi:10.1371/journal.pone.0009218 (2010).
80 Kim, S. W., Kim, S. J., Langley, R. R. & Fidler, I. J. Modulation of the cancer cell transcriptome by culture media formulations and cell density. *Int J Oncol* **46**, 2067-2075, doi:10.3892/ijo.2015.2930 (2015).
81 Shahdadfar, A., Fronsdal, K., Haug, T., Reinholt, F. P. & Brinchmann, J. E. In vitro expansion of human mesenchymal stem cells: choice of serum is a determinant of cell proliferation, differentiation, gene expression, and transcriptome stability. *Stem Cells* **23**, 1357-1366, doi:10.1634/stemcells.2005-0094 (2005).
82 Contoli, M. *et al.* Th2 cytokines impair innate immune responses to rhinovirus in respiratory epithelial cells. *Allergy* **70**, 910-920, doi:10.1111/all.12627 (2015).
83 McCollum, A. M. *et al.* Molluscum contagiosum in a pediatric American Indian population: incidence and risk factors. *PLoS One* **9**, e103419, doi:10.1371/journal.pone.0103419 (2014).
84 Borkar, D. S. *et al.* Association between atopy and herpetic eye disease: results from the pacific ocular inflammation study. *JAMA Ophthalmol* **132**, 326-331, doi:10.1001/jamaophthalmol.2013.6277 (2014).
85 Seneschal, J., Clark, R. A., Gehad, A., C.M., B.-A. & T.S., K. Human epidermal Langerhans cells maintain immune homeostasis in skin by activating skin resident regulatory T cells. *Immunity* **36**, 873-884 (2012).
86 Kim, M. *et al.* Relay of herpes simplex virus between Langerhans cells and dermal dendritic cells in human skin. *PLoS Pathog* **11**, e1004812, doi:10.1371/journal.ppat.1004812 (2015).
87 Puttur, F. K. *et al.* Herpes simplex virus infects skin gamma delta T cells before Langerhans cells and impedes migration of infected Langerhans cells by inducing apoptosis and blocking E-cadherin downregulation. *J Immunol* **185**, 477-487, doi:10.4049/jimmunol.0904106 (2010).

88 Petermann, P. *et al.* Entry mechanisms of herpes simplex virus 1 into murine epidermis: involvement of nectin-1 and herpesvirus entry mediator as cellular receptors. *J Virol* **89**, 262-274, doi:10.1128/jvi.02917-14 (2015).

Figure Legends:

Figure 1. Changes in Langerhans' cell core transcriptional network induced by epidermal cytokines are associated with a dramatic change in expression of IRF1, 4, and 8. a) Freshly isolated 48h migratory human LCs are CD1a/HLADR^{high}. **b)** The core transcriptomic networks of human LCs comprising 17 clusters, including 2 biggest clusters (01 and 02) of genes involved in antigen processing. Transcript-to-transcript clustering, (BioLayout *Express*^{3D}, r=0.85; MCL=1.7) of 527 probesets differentially regulated during 24 h of stimulation with TNFα and TSLP, maSigPro $p<0.05$. Lines (edges) represent the similarity between transcript expressions; circles (nodes) represent transcripts. Clusters of co-expressed genes are coded by colour. **c)** Expression profile of clusters 01 (95 genes) and 02 (85 genes) during 24 h stimulation with epidermal cytokines, green: TNFα, red: TSLP) d) Expression changes of *IRF1*, *IRF4* and *IRF8* in LC during the time course of stimulation with TNFα and TSLP, n=3 independent skin donors e) Differential induction of *IRF1* and *IRF4* mRNA by TNFα and TSLP during LC migration from biopsies (qPCR, cells from four 6 mm skin biopsies, n=6 in duplicate, mean ± SEM, $p<0.0001$ for IRF1 and IRF8, and 0.013 for IRF4, two-way repeated measurements paired ANOVA).

Figure 2. Network of IRF and their transcription partners regulates transcriptional programmes of dendritic cells

Model of IRF-GRN assembled based on a systematic literature review have been simulated with Signalling Petri Nets in BioLayout *Express*^{3D} Representative results of in silico simulation of the IRF network, measured at each of the output nodes, when *IRF1* only (dotted red), *IRF8* (blue), *IRF4* only (green), *IRF4* and AP1-binding TF (orange), *IRF4* and ETS-binding TF (dotted purple), *IRF1* and *IRF8* (grey) and *IRF1* and *IRF4* (turquoise) are expressed.

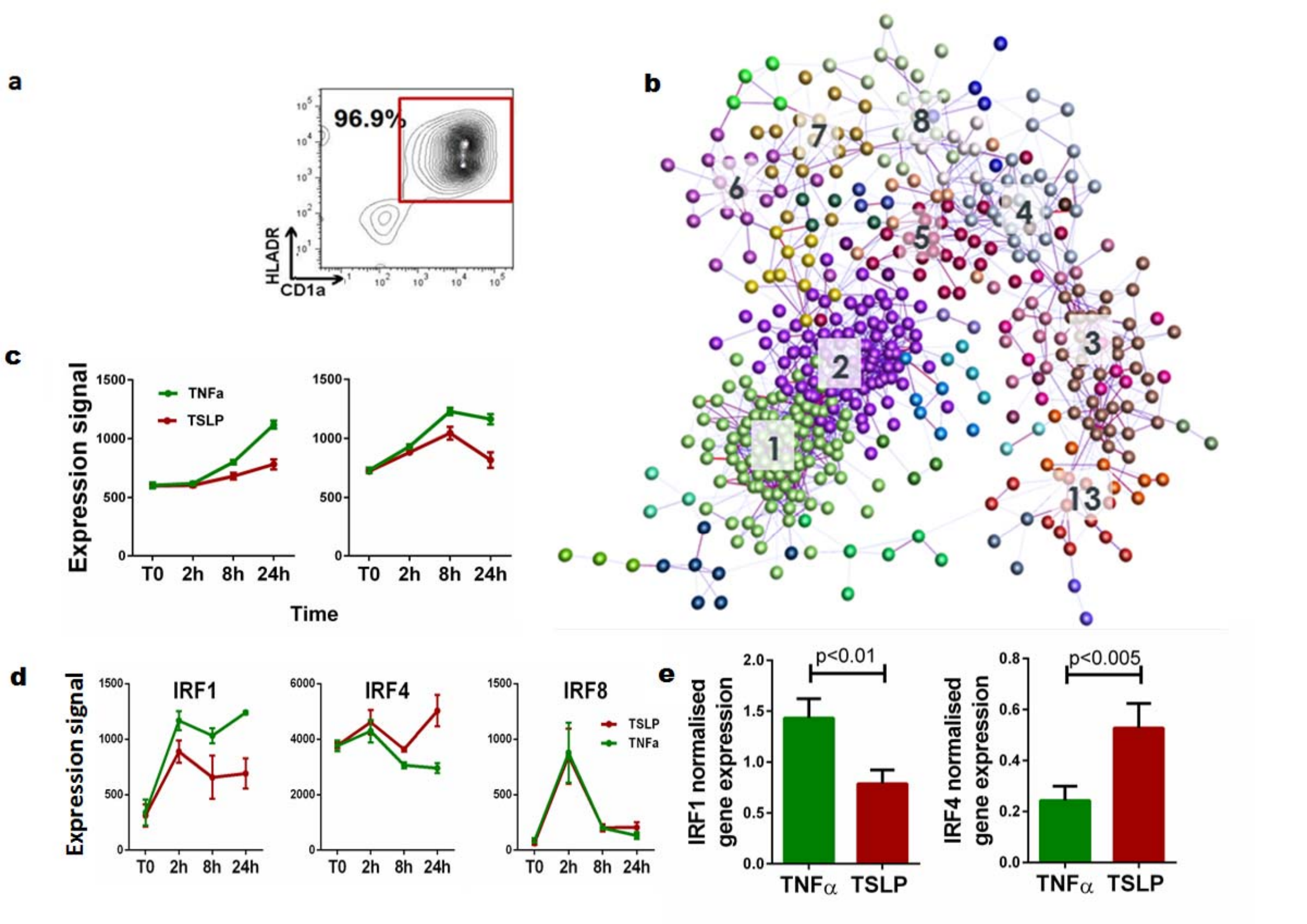
a
96.9%
HLADR
CD1a
b
1
2
3
4
5
6
7
8
13
c
Expression signal
TNFa
TSLP
T0 2h 8h 24h
Time
d
IRF1
IRF4
IRF8
TSLP
TNFa
e
IRF1 normalised gene expression
p<0.01
TNFα TSLP
IRF4 normalised gene expression
p<0.005
TNFα TSLP

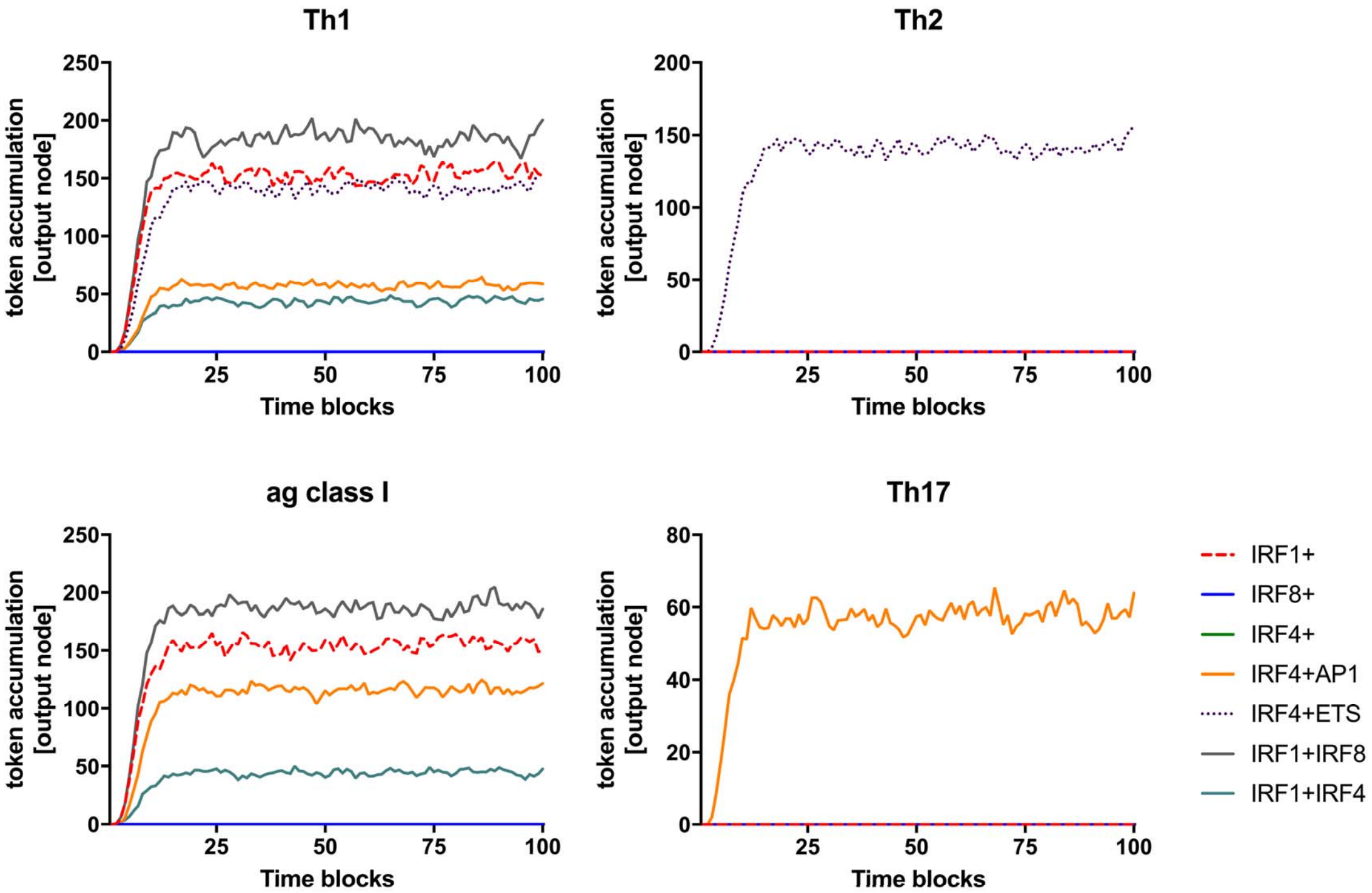
Th1
token accumulation [output node]
250
200
150
100
50
0
25
50
75
100
Time blocks
Th2
token accumulation [output node]
200
150
100
50
0
25
50
75
100
Time blocks
ag class I
token accumulation [output node]
250
200
150
100
50
0
25
50
75
100
Time blocks
Th17
token accumulation [output node]
80
60
40
20
0
25
50
75
100
Time blocks
IRF1+
IRF8+
IRF4+
IRF4+AP1
IRF4+ETS
IRF1+IRF8
IRF1+IRF4

Figure 3. Network of IRF and their transcription partners underpins biological function of human Langerhans cells.

Interferon Regulatory Factors gene regulatory network (GRN) in DCs, assembled basing on the systematic literature review, depicting *IRFs*, transcription partners, DNA sequences and transcribed genes arranged in columns from left to right. Components of the GRN are represented by rectangles (gene transcripts) and triangles (DNA sequences) connected by arrows representing molecular interactions (blue arrow: synergism, red arrow: inhibition). Green circle denotes binding. GRN output (i.e. immunological function) is presented in octagons on the right side of the diagram. The diagram is drawn in a Petri Net notation, where the interacting elements of GRN (nodes, gene transcripts) are interspaced with transitions (vertical black lines, and black diamonds). Input nodes: *IRF* 1,4, and 8, and transcription partners grouped as ETS or AP-1 family. Assumption: IRF can bind with any TP from the ETS family. There are 28 members of ETS family, and 5 AP-1 binding transcription factors. Only the transcription partners exceeding 150 RMA normalised expression level in the human skin LC microarray dataset were included in the diagram. The nodes include (classes: left to right, list: top to bottom: Transcription factors: *IRF1*, *IRF8*, *IRF4*, IRF-binding partners: AP-1 family: *JUN*, *FOS*, *BATF*, *BATF3*, ETS family: *ELF1*, *ELF4*, *ELK1*, *ELK3*, *ETS1*, *ETS2*, *EHF*, *ELF2*, *ETV3*, *ETV6*, *GABPA*. DNA binding sequences: AICE, ISRE, EICE. Output genes: Programme A (bracket indicates output genes depicted in a single node): *CAV1*, *ERAP1,2, TAP1, (HLA A-F, B2M), TAP2, TAPBPL, PSME1, PSME2, PSMB10, CYBB, (CD40, CD80, CD86), IL15, IL12p40, IFNb, iNOS, IL18*. Programme B: *IL10, IL33, CD74, LYZ, CIITA, PRDM1*. Biological processes: Th17 responses, antigen presentation in class I, phagocytosis, Th1 responses, Th2 responses, antigen presentation in class II. Each interaction has been confirmed by two independent reports in myeloid cells. The diagram captures the combinatory nature of immune activation, depending on the levels of expression, timing and interactions between the regulatory elements. The flow of the signal through the diagram can be modelled mathematically using experimental or theoretical data and visualised in

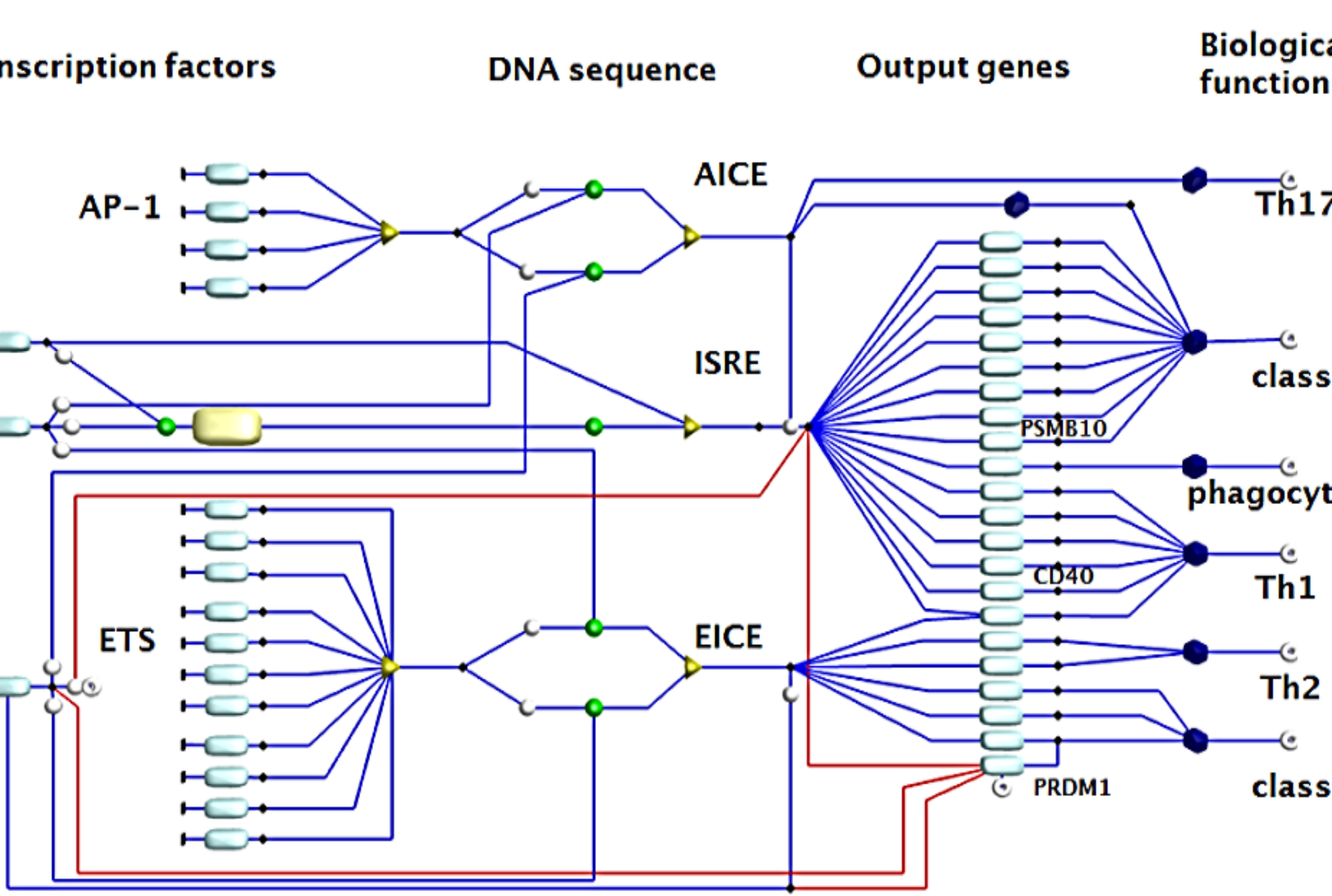
nscription factors
DNA sequence
Output genes
Biologica
function
AP-1
AICE
ISRE
ETS
EICE
PSMB10
CD40
PRDM1
Th17
class
phagocyt
Th1
Th2
class

BioLayout Express^{3D}. Programmes A (green) and B (red) are controlled by combinatorial binding of IRF-TP to different DNA sequences. The detailed diagram can be edited/downloaded from http://www.virtuallyimmune.org/irf-grn/.

Figure 4. *In silico* simulation of GRN predicts changes in expression of genes regulated by IRFs and the outcome of T lymphocyte stimulation by LCs.

a-f) Expression levels of *PSMB10* (a,b) *CD40* (c,d) and *PRDM1* (e,f) predicted in silico (a,c,e) and measured 24h post *in vitro* activation of LCs (b,d,f). **g,h)** The ability of TNFα (black) and TSLP (grey) matured LCs to stimulate antigen-specific CD8+ T cells was simulated *in silico* and measured in ELISpot in vitro assay. **g)** Result of in silico simulation of the IRF network, measured at the output node when the input nodes are marked as per the gene expression values during LCs stimulation with TNFα and TSLP, Signalling Petri Nets: BioLayout *Express*^{3D}, 100 time blocks, 500 runs. Number of tokens in the output node in the 10 final time blocks shown. **h)** Activation of antigen-specific CD8+ T cells by TNFα (grey) and TSLP (black) matured LCs, pulsed with a long peptide antigen requiring cross-presentation, IFN-γ production measured in co-culture ELISpot assay, n=6 in triplicate, mean +/- SE.

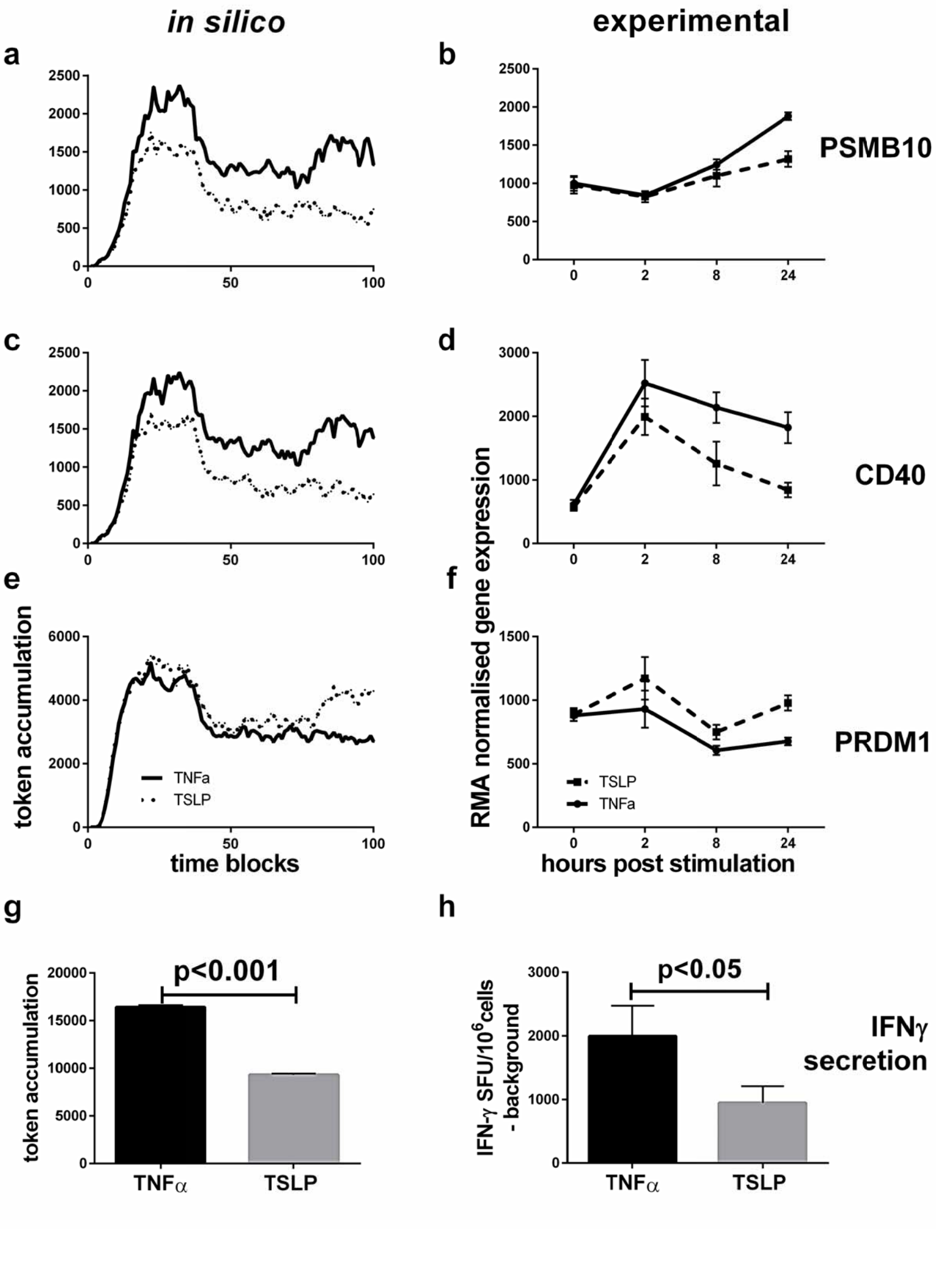
in silico
experimental
a
b
c
d
e
f
g
h
PSMB10
CD40
PRDM1
TNFa
TSLP
token accumulation
time blocks
RMA normalised gene expression
hours post stimulation
p<0.001
p<0.05
IFNγ secretion
IFN-γ SFU/10^6cells - background
TNFα

Petri Net computational modelling of Langerhans cell Interferon Regulatory Factor Network predicts their role in T cell activation.

Authors: Marta E. Polak, MSc, PhD*[1,2], Chuin Ying Ung[1], MD, Joanna Masapust[1], MSc, Tom C. Freeman, PhD[3,4] , Michael R. Ardern-Jones, BSc, FRCP, DPhil[1,4]

[1] Clinical and Experimental Sciences, Sir Henry Wellcome Laboratories, Faculty of Medicine, University of Southampton, SO16 6YD, Southampton, UK

[2] Institute for Life Sciences, University of Southampton, SO17 1BJ, UK.

[3] The Roslin Institute and Royal (Dick) School of Veterinary Studies, University of Edinburgh, Easter Bush, Edinburgh, Midlothian EH25 9RG, UK

[4] These authors contributed equally to this work

***Corresponding Author:**

Dr. Marta E. Polak,

Address: Clinical and Experimental Sciences, Faculty of Medicine, University of Southampton, Southampton General Hospital, LE59, MP813, SO16 6YD, Southampton, UK

Tel: 02381205727, e-mail: m.e.polak@soton.ac.uk

SUPPLEMENTARY MATERIALS AND METHODS

Assembly of the IRF GRN diagram

Components of the GRN are represented by rectangles connected by arrows indicating molecular interactions (blue arrow: synergism, red arrow: inhibition). GRN output (i.e. immunological function) is presented in octagons on the right side of the diagram. The diagram is drawn in a Petri Net notation, where the interacting elements of GRN (nodes, gene transcripts) are interspaced with transitions (vertical black lines, and black diamonds). The diagram captures the combinatory nature of immune activation, depending on the levels of expression, timing and interactions between the regulatory elements. The flow of the signal through the diagram can be modelled mathematically using experimental or theoretical data and visualised in BioLayout Express^{3D}. The abundance of a molecule at any given network node can be represented by the placement of tokens. Edges connecting the nodes and transitions determine the direction of the token flow through the diagram, representing the progress of the biological process.

The network assembly has been done in the following steps:

Introducing network components (rectangles, nodes) and interactions (black diamonds, transitions):

a. Input nodes: IRF 1,4, and 8, and transcription partners grouped as ETS or AP-1 family. Assumption: IRF can bind with any TP from the ETS family. There are 28 members of ETS family, and 5 AP-1 binding transcription factors. Only the transcription partners exceeding 150 RMA normalised expression level in the human skin DC microarray dataset were included in the diagram.

b. DNA binding sequences: EICE, ISRE, AICE

c. Genes controlled by each IRF or IRF-TP heterodimer (ChIP-seq data, only the genes exceeding 150 RMA normalised expression level in the human skin DC microarray dataset and related to activation of T cell activation by DCs were included in the diagram).

d. Output nodes (octagons): Regulated genes

e. Output nodes (octagons): Biological processes

f. Interactions: black diamonds

Connecting the network components with edges to represent the identified interactions.

a. IRF, IRF TP, and corresponding DNA binding sequence were connected with stimulatory edges (black arrows) including all possibilities detailed in the Table S3 (e.g. IRF8 can bind to EICE with ETS, to AICE with AP-1 or ISRE with IRF1), preserving the and/or logic (i.e. IRF8 cannot bind to ISRA without IRF1: transition "and", IRF 1 can connect to ISRA either on its own or hetero-dimerised with IRF8: transition "or"). The Boolean logic gates "and" and "or" have been recreated using two nodes to transition ("and") and two transition to node ("or") (Signal flow through "and" ad "or" gate is presented in Figure S2)

f. Genes identified by ChIP-seq analysis of IRF1,4, and 8 were associated with the DNA binding sequence, and with the output biological process. Assumption: controlling IRF homo/heterodimer determines DNA binding sequence. If a gene can be controlled by two transcription factors/two DNA sequence (e.g. IL18 via IRF1 or IRF8/ETS complex) both possibilities were included in the diagram.

Adding entry transitions for input nodes: (transitions: black bars)

a. An entry transition was added before each entry node to allow setting up initial marking of the network and input of the numerical data.

Converting diagram edges into appropriate interactions (stimulatory: black arrows, inhibitory: red open diamonds)

a. Each edge drawn is initially a black stimulatory edge. To convert the interaction to an inhibitory, the arrow was replaces with an open diamond shape end. For clearer visualization the inhibitory edges are colored red.

SUPPLEMENTARY FIGURE LEGENDS

Figure S1. Regulation of transcription factor expression in human LCs by epidermal cytokines.

A list of probesets encoding transcription factors filtered to contain one probeset per gene, and above 150 expression value have been curated from the whole transcriptome dataset, using and the transcription factors activated during LC activation with epidermal cytokines were identified using (LIMMA,(*28*)). Expression values (a,b, d,f) and fold change differences (c,e,g) are visualised for top transcription factors expressed at base line (a) up-regulated (b-e) and differentially regulated (f,g) by epidermal cytokines are shown. T0 DDC used for comparison in (a) have been isolated as previously published {Polak, 2014 #2259}.

Figure S2. Network of IRF and their transcription partners regulates transcriptional programmes of dendritic cells.

a) Model of Interferon Regulatory Factors gene regulatory network (GRN) in LCs, assembled based on a systematic literature review, depicting; IRF, transcription partners, DNA sequences and transcribed genes arranged left to right. Each interaction has been confirmed by two independent reports in myeloid cells. Components of the GRN are represented by rectangles connected by arrows representing molecular interactions (black arrow: synergism, red arrow: inhibition). GRN output (i.e. immunological function) is presented in octagons on the right side of the diagram. The diagram is drawn in a Petri

net notation, where the interacting elements of GRN (nodes, gene transcripts) are interspaced with transitions (vertical black lines, and black diamonds). The diagram captures the combinatory nature of immune activation, depending on the levels of expression, timing and interactions between the regulatory elements. The flow of the signal through the diagram can be modelled mathematically using experimental or simulated data and activity flow visualised in BioLayout Express3D.

b-e) Effect of signal transmission through "and" and "or" Boolean gates

Petri Net network motifs demonstrating the principles of signal flow through "and" (b,d) and "or" (c,e) gates with input from single (b,c) and multiple (d,e) transitions. Initial network marking = 100, token accumulation after gate are shown in the right column, 100 time blocks, 500 runs, simulation under the conditions of standard distribution.

Figure S3: Genes expression profiles in transcriptional programmes "A" and "B" match the *in silico* prediction

a) *In silico* profiles of gene expression in programmes "A" and "B" , measured at the output node when the input nodes are marked as per the gene expression values during LCs stimulation with TNF-α and TSLP, Signalling Petri Nets: BioLayout *Express*3D, 100 time blocks, 500 runs. **b**) Expression profiles of individual genes in "Programme A" as measured in the microarray experiment. **c**) Expression profiles of individual genes in "Programme B" as measured in the microarray experiment.

Figure S4: Ability of LC to cross-present antigens is modified by TNFα and TSLP.

Activation of antigen-specific CD8+ T cells by medium (white), TNFα (grey), TSLP (black) and a combination of TNFα and TSLP (black checkerboard grey) matured LCs, pulsed with a long peptide antigen requiring cross-presentation, IFN-γ production measured in co-culture ELISpot assay, n=2 in triplicate, mean +/- SE.

Figure S5: Effect of PI3K-γ inhibitor on the ability of LC migrating from epidermal biopsies to polarise naïve CD4 T cell responses.

Human epidermal biopsies (a) were exposed to PI3Kγ inhibitor or control media for 48h. The ability of migratory LCs (b) to polarise adaptive immune responses was predicted *in silico* (c,d, BioLayout Express3D, 100 time blocks, 500 runs) and measured in vitro (e,f) IFNγ (e) and IL-4 (f) measured by Elispot, n=6, in triplicate, mean ± SEM shown. Control media (black bars) or PI3Kγ inhibitor [1μMol] (grey bars). Experimental p values: Paired t-test for means

SUPPLEMENTARY TABLES

Table S1: Search strategy to identify components of the IRF GRN network

Table S2: Interaction database

Table S3: Boolean gates

Table S4: Genes regulated by IRF1,4 and 8: ChIP-seq analysis

Table S5: Genes regulated by expression programme "A" and "B" in the IRF-GRN

Table S6: Experimentally measured expression values at 0h (0-8 time block),2h (9-32 time block),8h (33-75 time block),and 24h (76-100 time block) converted to parametrisation values for each GRN entry nodes.

Table S7: Experimentally measured expression values for input nodes in LC migrating in the presence or absence of PI3K-gamma inhibitor, AS605240, average of n=2.

Supplementary Figure 1

a Top 40 TF expressed in LCs at T0

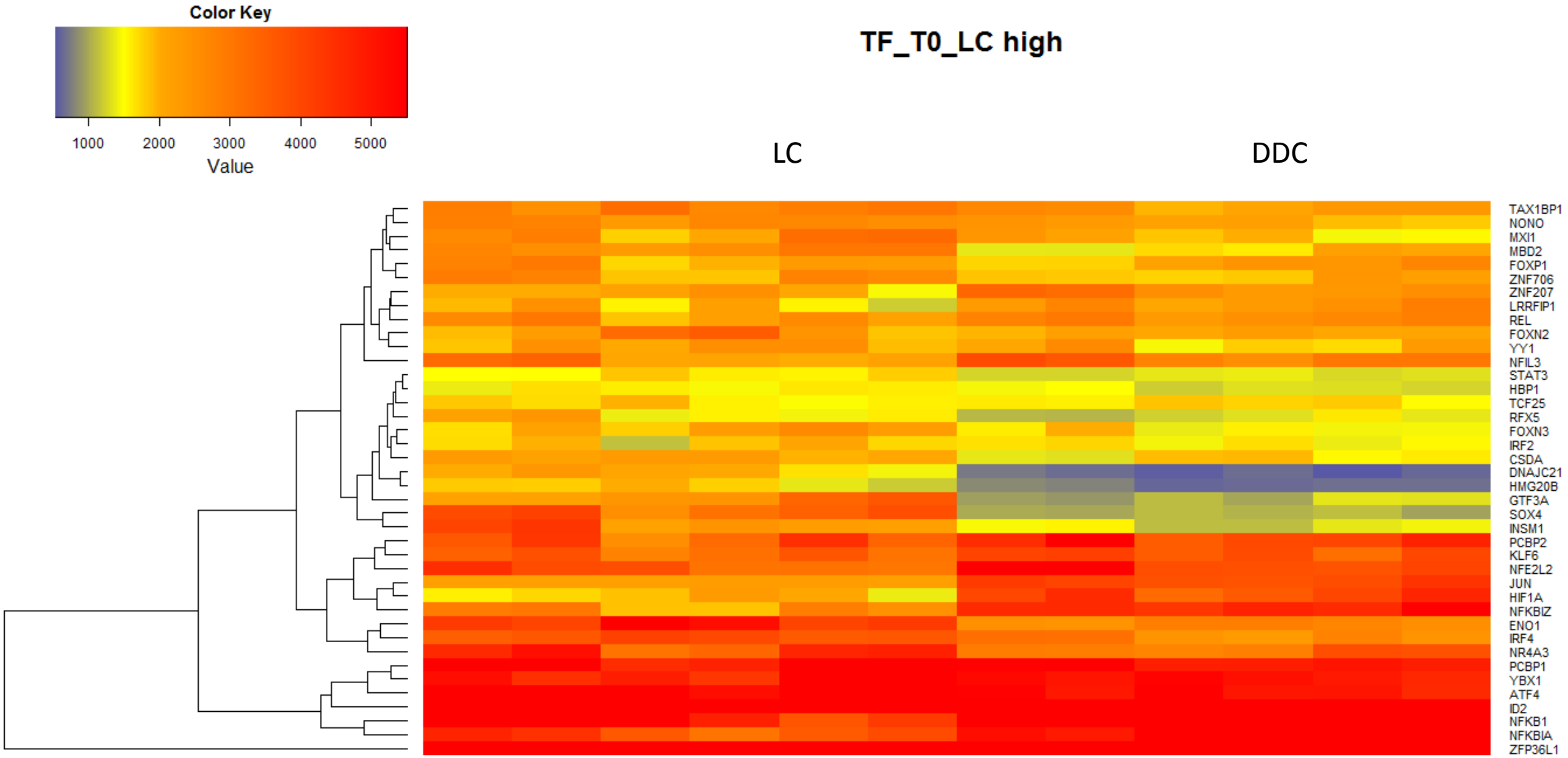

Supplementary Figure 1

b Top 40 TF up-regulated in LCs at 2h stimulation with TNFa

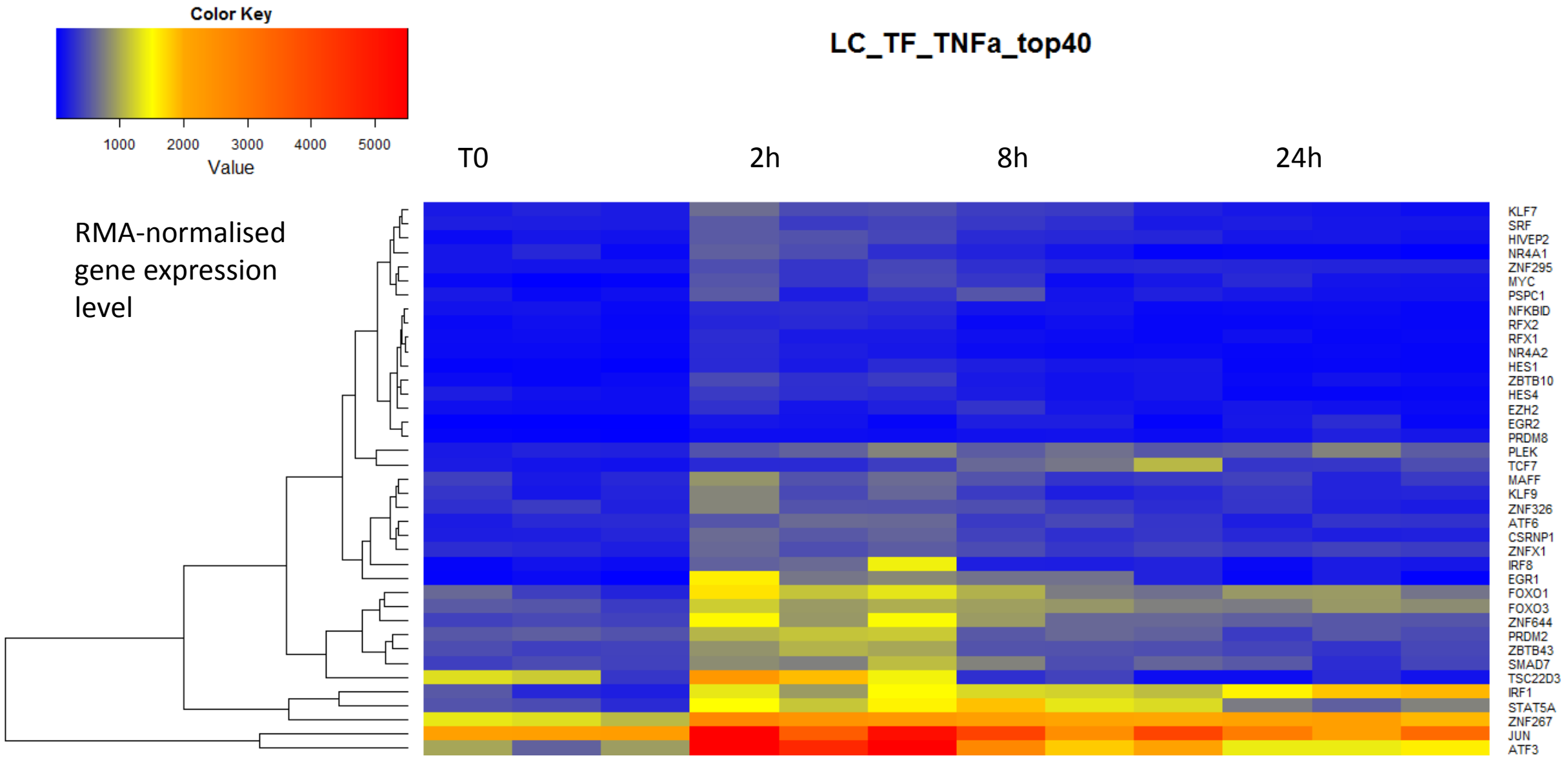

Supplementary Figure 1

c Top 40 TF up-regulated in LCs at 2h stimulation with TNFa

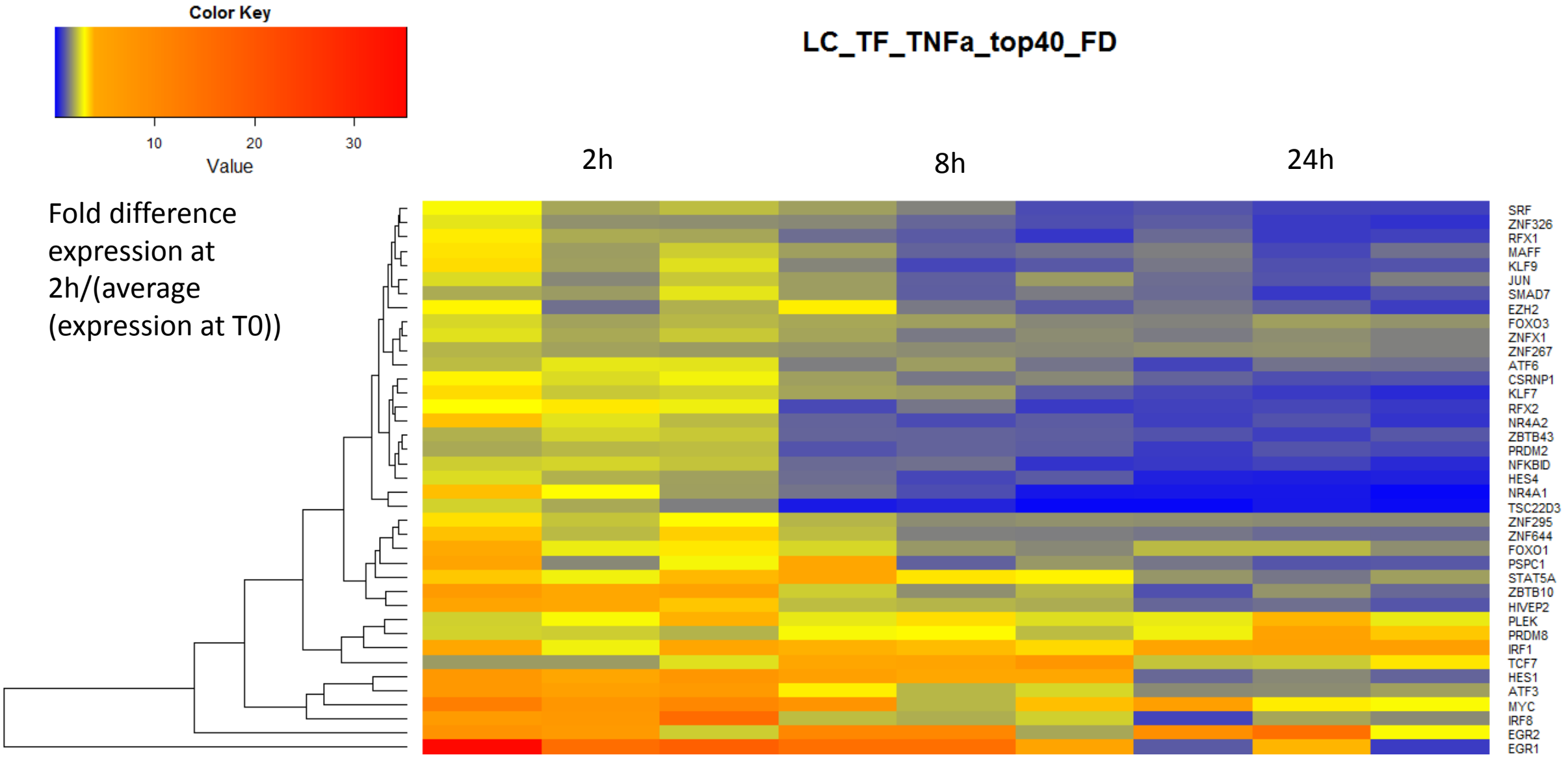

Supplementary Figure 1

d Top 20 TF induced by TNFa & Top 20 TF induced by TSLP

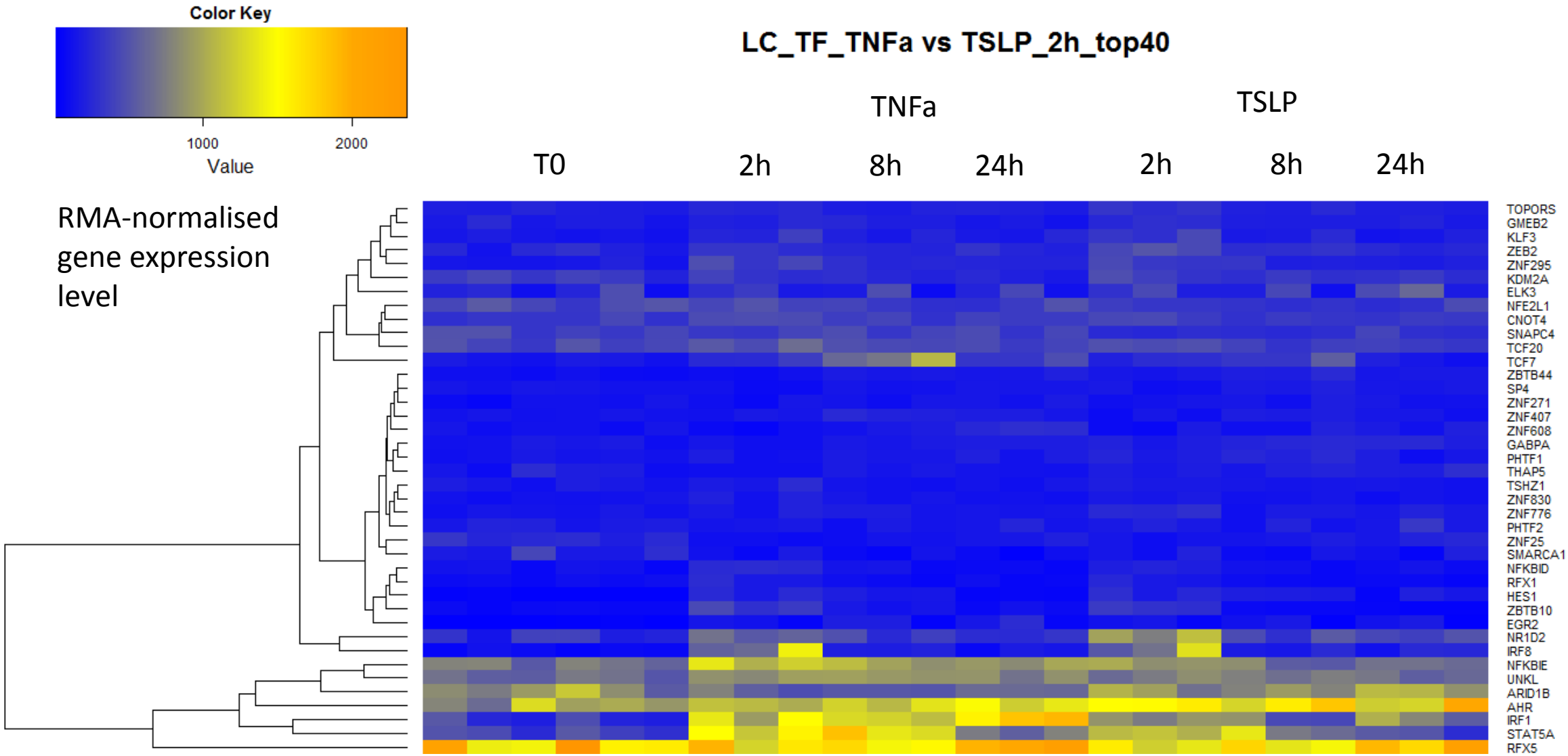

Supplementary Figure 1

e Top 20 TF induced by TNFa & Top 20 TF induced by TSLP

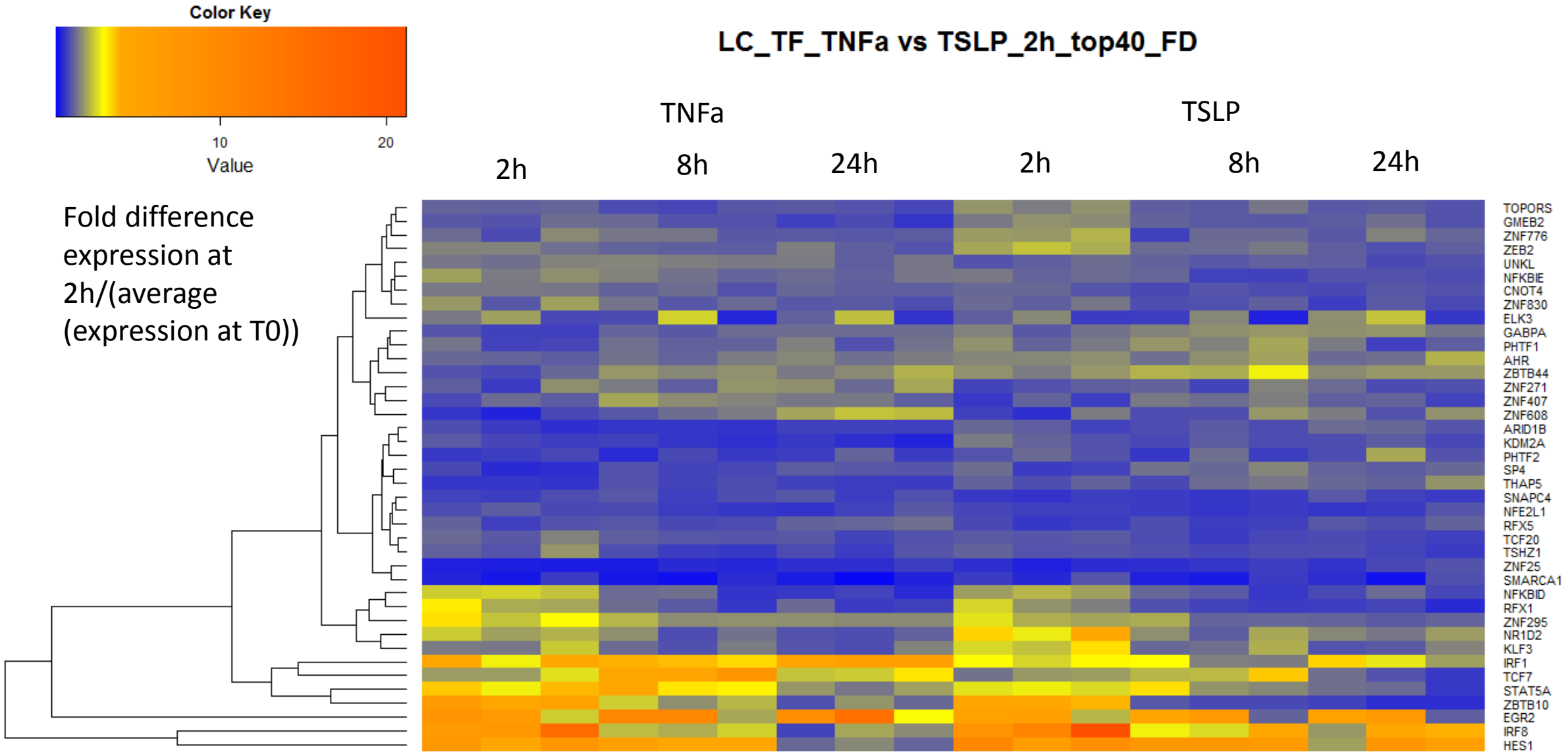

Supplementary Figure 1

f Top 20 TF induced by TNFa & Top 20 TF induced by TSLP

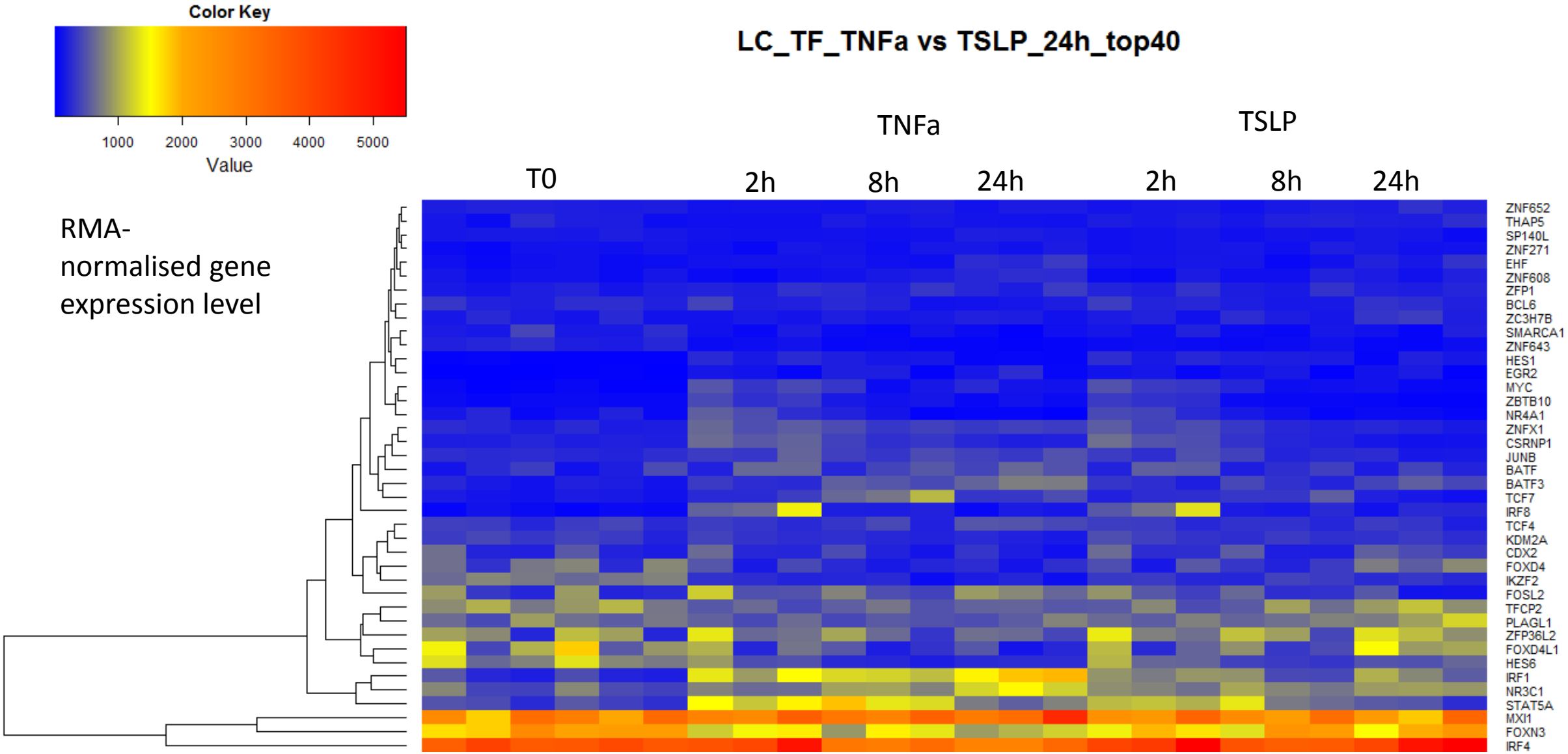

Supplementary Figure 1

g Top 20 TF induced by TNFa & Top 20 TF induced by TSLP

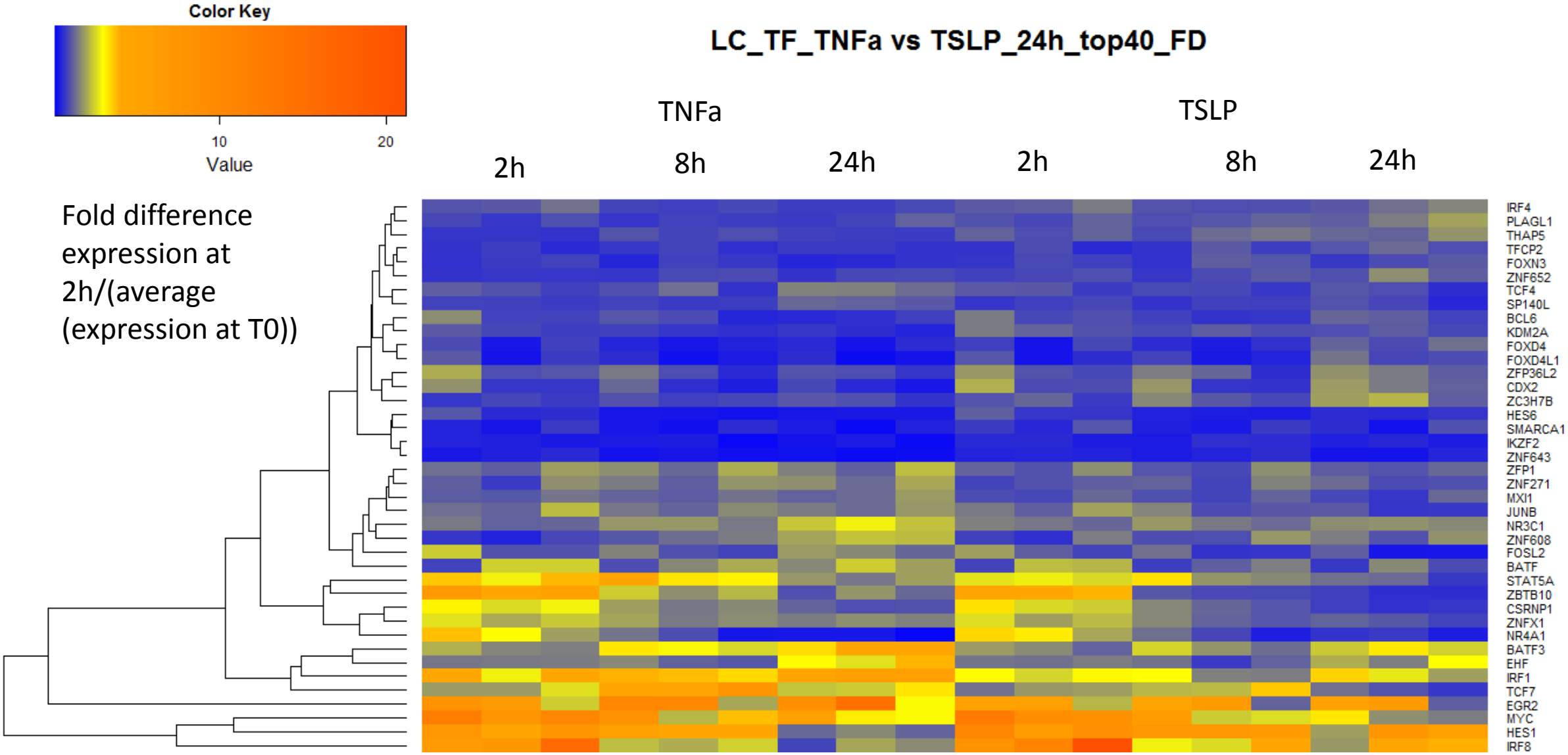

Supplementary Figure 2. Network of IRF and their transcription partners regulates transcriptional programmes of dendritic cells.

a

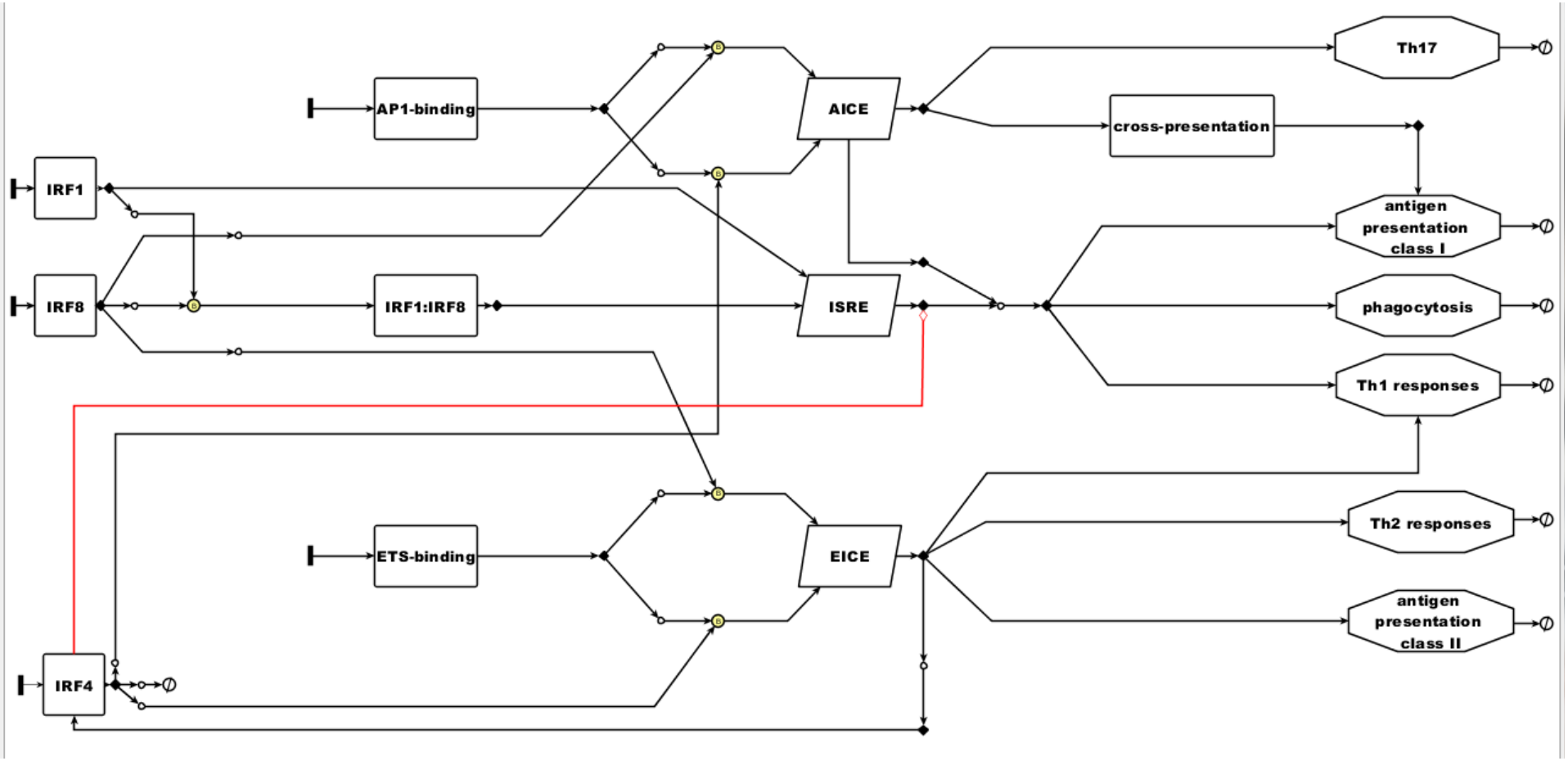

Supplementary Figure 2: Boolean networks: and/or gates

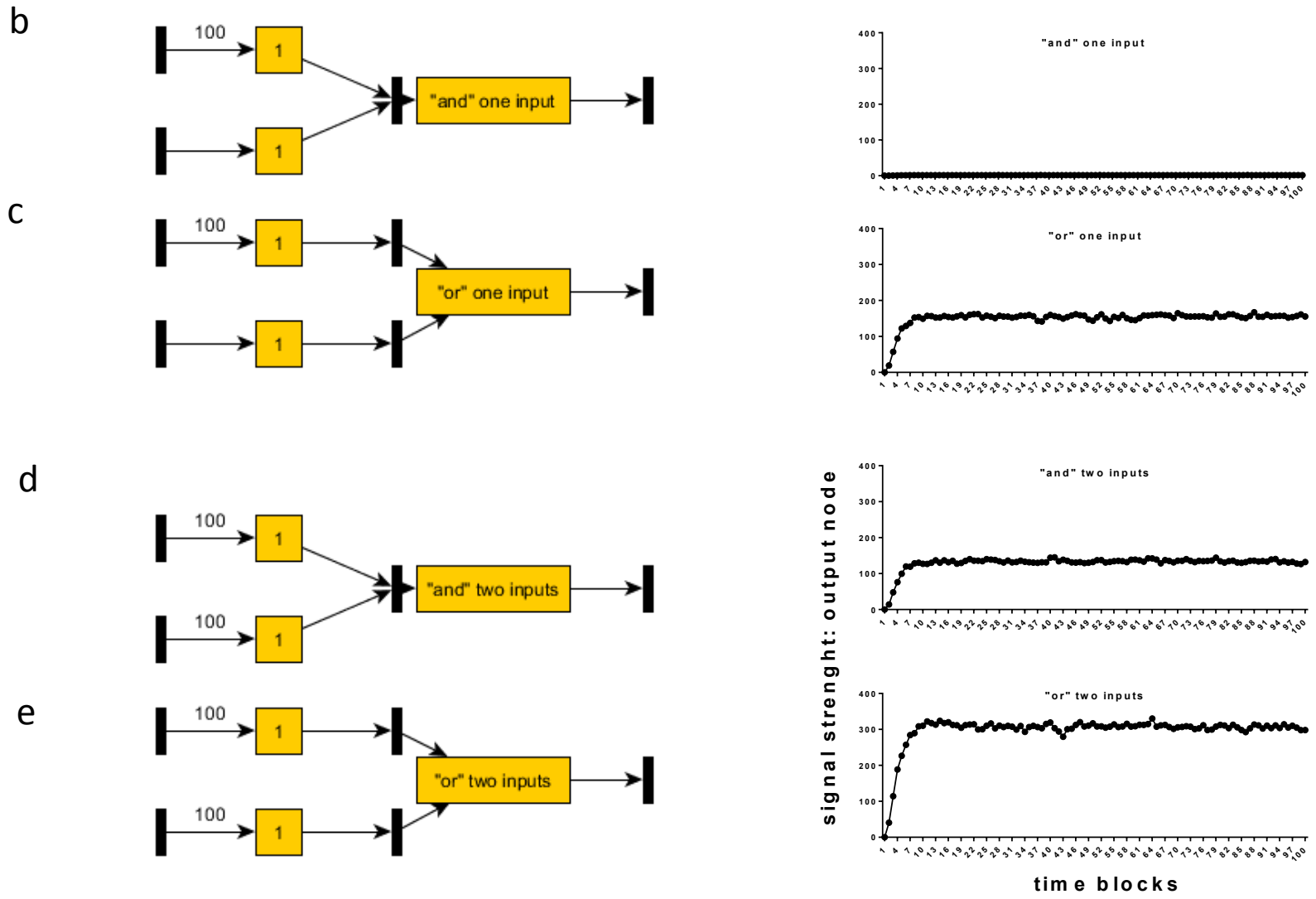

Supplementary Figure 3:
In silico profiles of genes involved in programme “A” and “B”

a

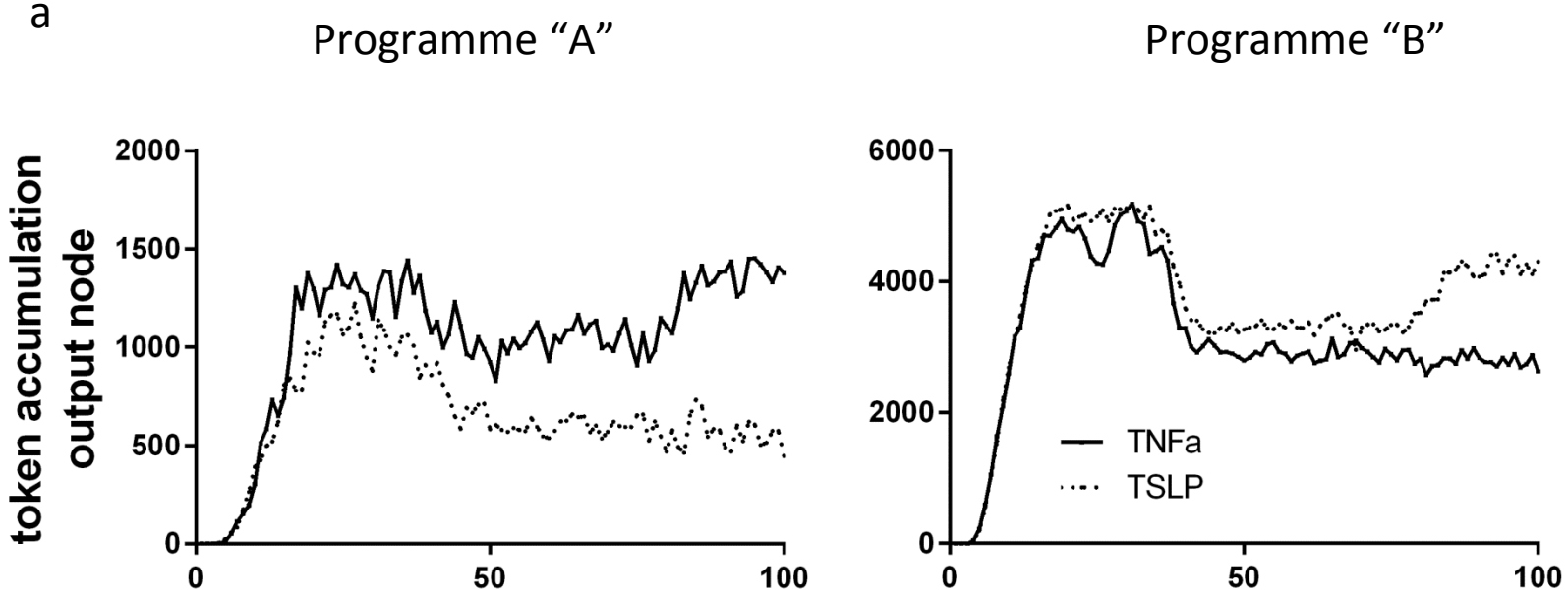

b

Programme “A” : genes up-regulated by TNF-α

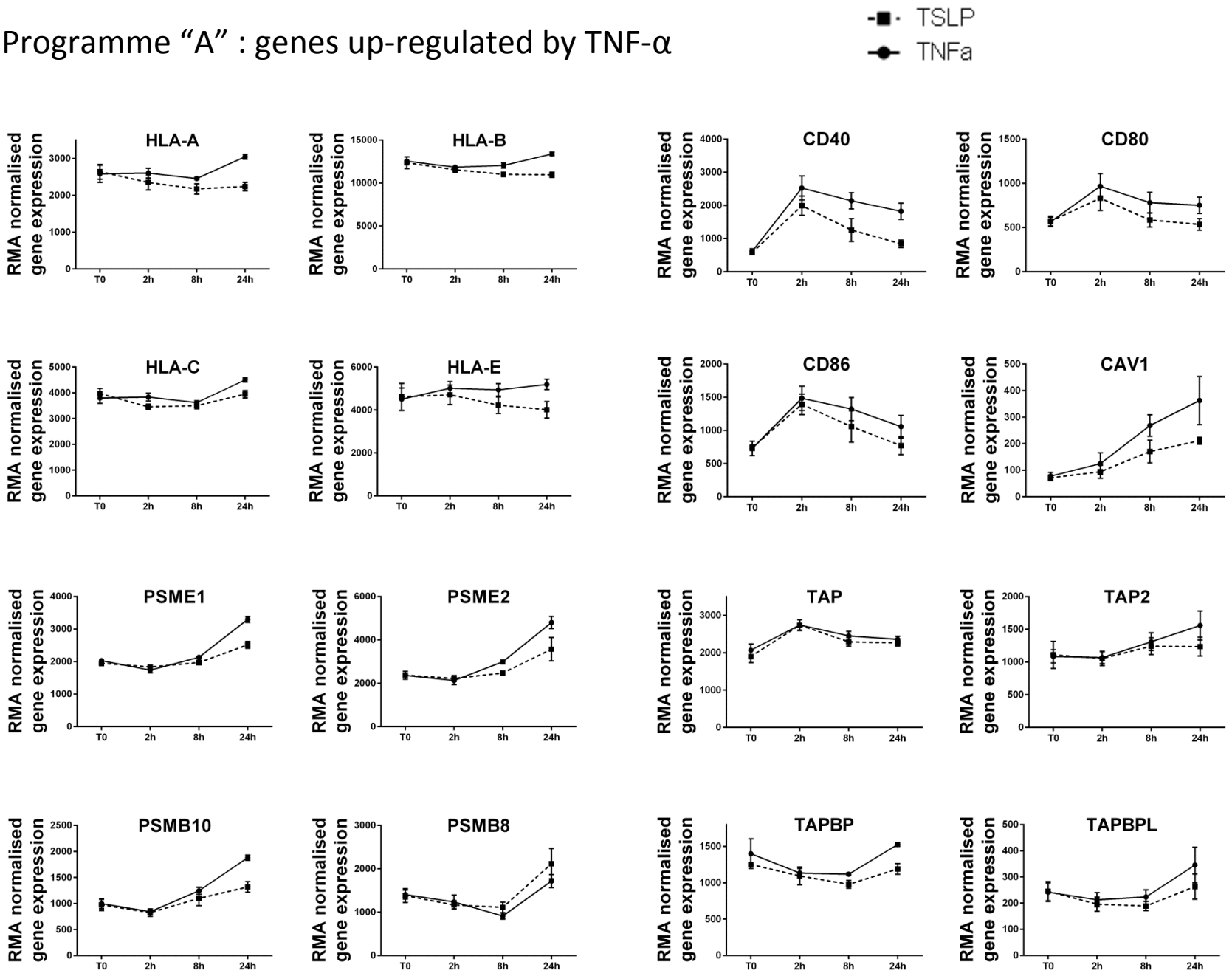

C

Programme “B” : genes regulated in simillar manner by TNF-α and TSLP

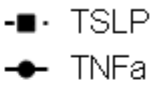

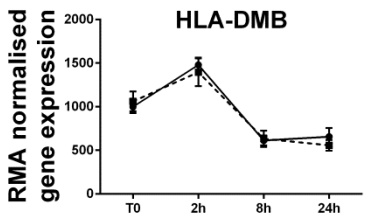

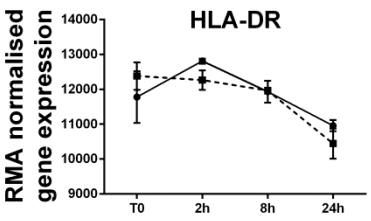

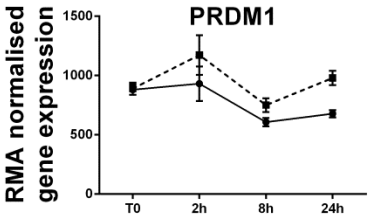

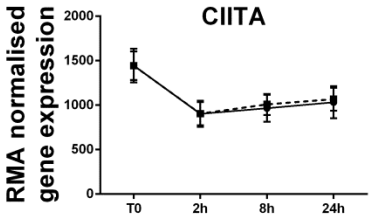

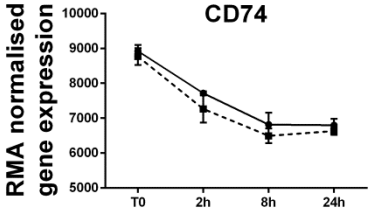

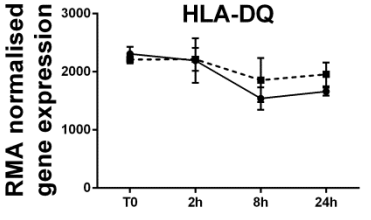

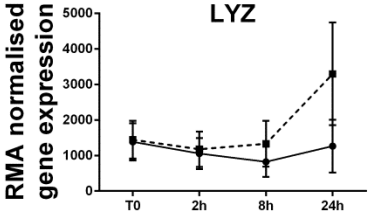

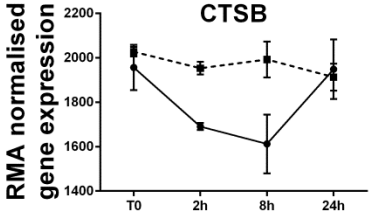

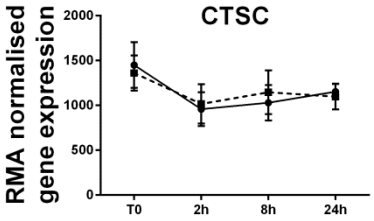

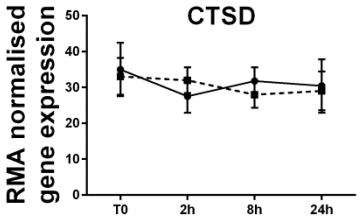

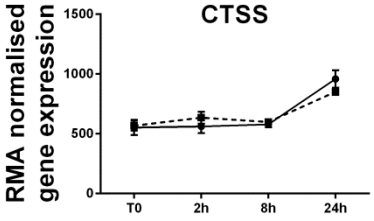

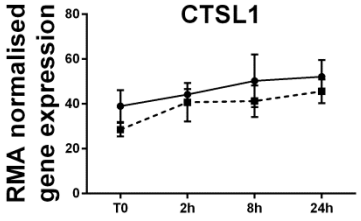

cytokines

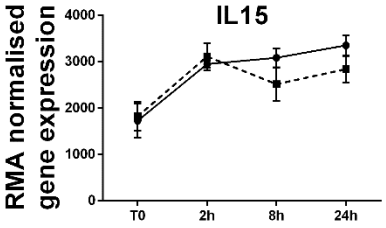

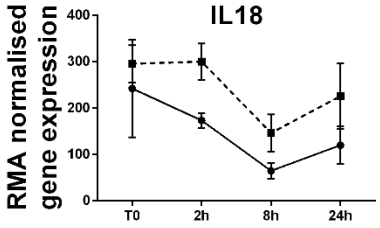

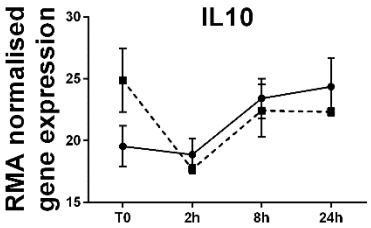

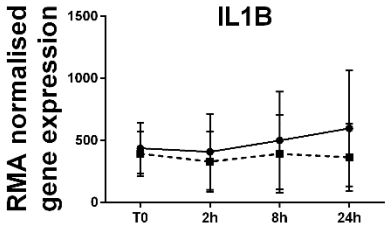

ERAP

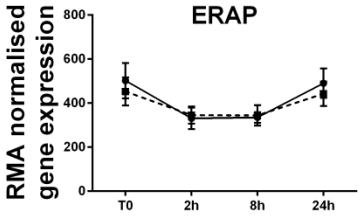

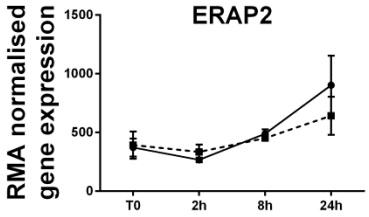

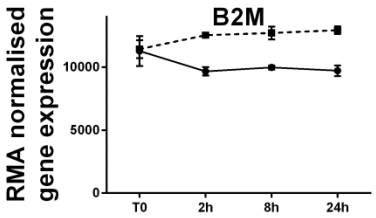

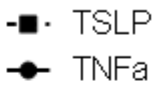

Supplementary Figure 4. Ability of LC to cross-present antigens is modified by TNFα and TSLP.

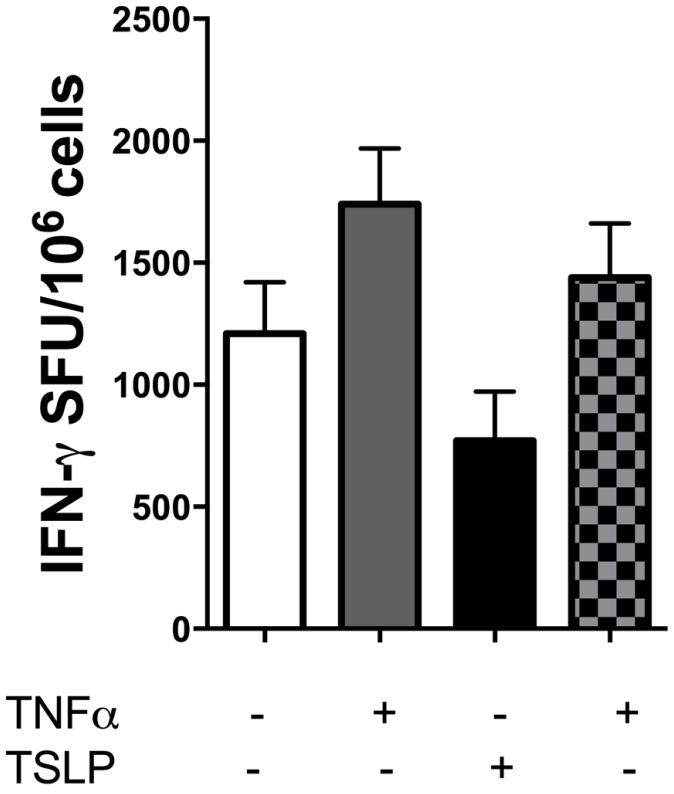

Supplementary Figure 5. Effect of PI3Kγ inhibitor on the function of LC migrating from epidermal biopsies.

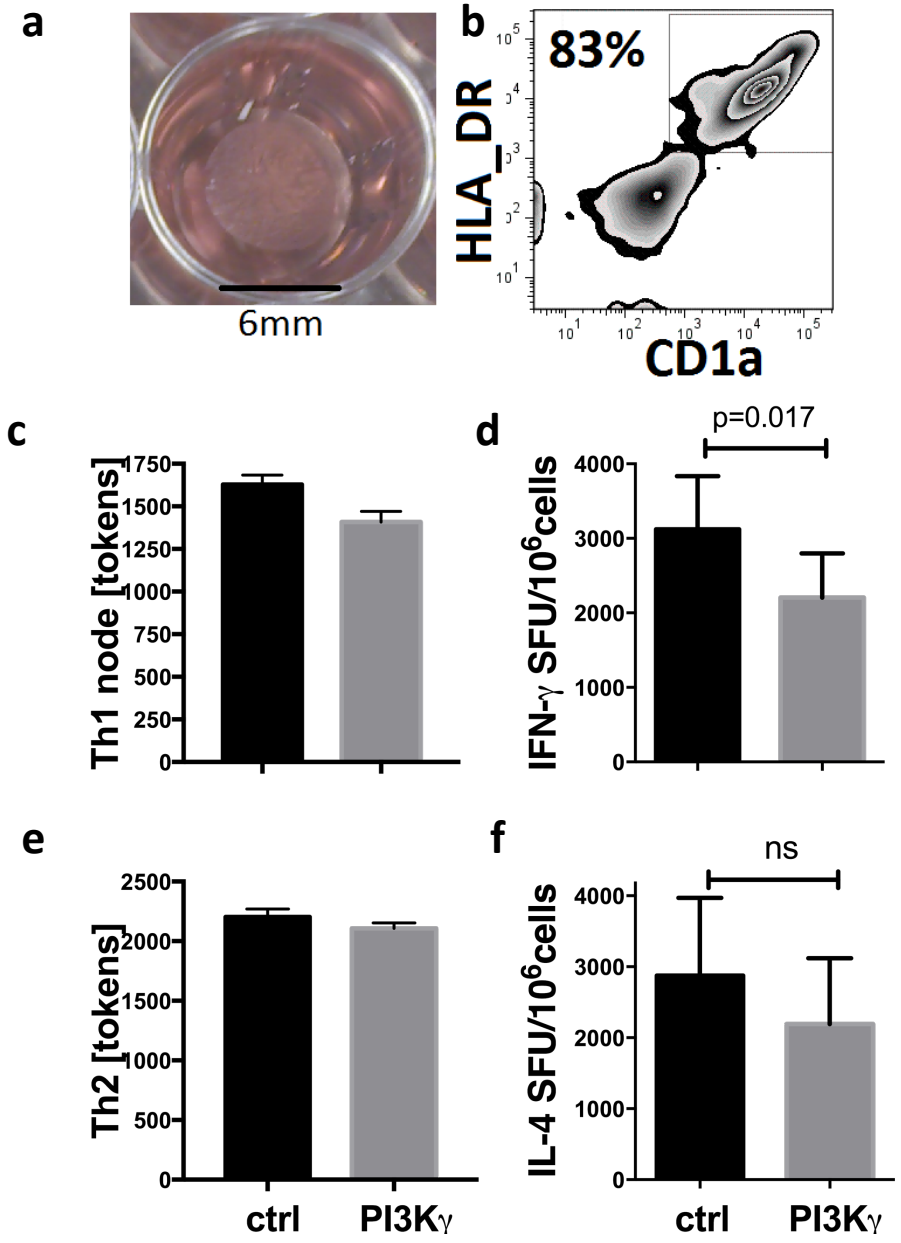

Table S1. Search strategy to identify components of the IRF GRN network

search term	number of publications
"Interferon regulatory factor" or IRF and antigen presentation	71
"Interferon regulatory factor" or IRF and dendritic cell and T cell stimulation	22
"Interferon regulatory factor" or IRF1 or IRF4 or IRF8 and *transcripton partner* as per the transcription partner list	510
Interferon regulatory factor or IRF1 or IRF4 or IRF8 and ChIP-seq	15

Table S2. Interaction database

Citation	pubmed id	cell type	Stimulus	partner A	interaction	Partner B	DNA sequence	outcome
Hildner Science 2008	19008445	DC (mouse)		BATF3	essential			cross-presentation
Hildner Science 2008	19008445	DC (mouse)		BATF3	essential			anti-viral responses
				BATF3		IRF4/8???	AICE?	cross-presentation and CD8 responses
Ma JBC 1997	9099678	nucleic acid level	IFNg priming for LPS	ETS2		?	ETS2 - site, complex F1	IL12p40
				ETS2		?		IL12p40+>Th1
Roy JI 2015	25957166	macrophages	IFNg	IRF1	synergy	BATF2	IRF1 binding	Th1
Marecki JI 2001	11359842	fibroblasts (transf)		IRF1	synergy	IRF4/PU.1	ISRE/EICE	IL1B
Marecki JI 2001	11359842	fibroblasts (transf)		IRF1	synergy	IRF8/PU.1	ISRE/EICE	IL1B
Shi Gene 2001	21803131	monocytes		IRF1				antigen processing to class I
Gabrielle J Leukocyt Biol 2006	16966383	DC (mouse)		IRF1		inhibits		immunological tolerance
Gabrielle J Leukocyt Biol 2006	16966383	DC (mouse)		IRF1	essential	essential		immunological activation - CD8 Th1
Casola J Virol 2001	11413310	RSV infected alveoral epithelial cells		IRF1			ISRE	CCL5
Elser Immunity 2002	12479817	T cells		IRF1	inhibitory		IRFB, A, C sites (IL-4 pror	suppression of IL4
Karmann J Exp Med 1996	8691131	HUVEC	CD40, TNFa, IL1b	IRF1		??ATF-2/cJun/CREB		VCAM1, ICAM1,MHC class I
Kirchhoff FEBS 1999	10215868			IRF1		NFkB	PRD1-3, not 4	IFN-b
Fujita Nature 1989	2911367			IRF1			PRD1, PRD3	IFN-b
Fujita PNAS 1989	2557635		IFNg, TNFa, IL1, PolyI:C	IRF1				IFN-b
Kumatori JBC 2002	11781315			IRF1		STAT1	-100 GAS & -88 ISRE	gp91 phox
Eklund JI 1999	8805641			IRF1				gp91 phox
Saura J Mol Biol 1999	10356322	macrophage line (mouse)	IFNg and TNFa	IRF1	physical change of prom	NFkb		iNOS
Dror Mol Immunol 2007	16597464	macrophages		IRF1	binding	IRF8		Th1
Dror Mol Immunol 2007	16597464	macrophages		IRF1	binding	IRF8		iNOS
Gabrielle J Leukocyt Biol 2006	16966383	DC (mouse)		IRF1 null	essential			immunological tolerance
Masumi Mol Cell Biol	10022868	Mo/MF lines		IRF1, IRF2	essential	PCAF	ISRE	endogeneous IRF (only 1 and 2) recruit histone acetylases to enhance transcription
Masumi Mol Cell Biol	10022868	Mo/MF lines		IRF1, IRF2	essential	CBP/p300	ISRE	
Masumi Mol Cell Biol	10022868	Mo/MF lines		IRF1, IRF2	essential	GCN5	ISRE	
interaction				IRF1	essential and sufficient for ISRE and Th1		ISRE	Th1
interaction				IRF1	essential and sufficient for ISRE and CD8		ISRE	CD8 Tcells/ag presentation in class I
Marecki JI 2001	11359842	macrophages	LPS	IRF4		PU.1		IL1B
Marecki JI 2001	11359842	macrophages	IFNg+ LPS	IRF4		PU.1		IL1B
O'Reily JBC 2003	12676954	macrophages		IRF4		PU.1		repression of CD68
Ahyi JI 2009	19592658	T cell (mouse)		IRF4		PU.1 ?		Th2 - low cytokines
Glasmacher Science 2012	22983707			IRF4		BATF in the absence of P	AICE	Th17
Matsuyama Nucl Acid Res 1995	7541907		antigen-receptor interac	IRF4			ISRE	MHC class I
Brass 1996	8824592	B cells		IRF4		PU.1	EICE	induces B cell differentiation
Brass 1996	8824592	B cells		IRF4				represses IFN-inducible proliferation
Eisenbeis 1995	7797077	B cells		IRF4		PU.1	ISRE/EICE	mutual co-activation
Escalante 2002	12372320			IRF4		PU.1	AAxxGGAA IECS/EICE?	mutual co-activation
Kwon Immunity 2009	20064451	T cells	IL21	IRF4		STAT3	TTTC	PRDM1 (BLIMP1, T cell differentiation)
Honma PNAS 2008	18836070	T cell (naive)	TCR	IRF4	competition	IRF1	competitive	programming of Th responses
Yamagata 1996	8657101	T cells		IRF4	suppression	IRF1	GAGGAAACGAAACC	binding, suppression of IRF1
Li Nature 2012	22992523	T cells	IL21, CD3-CD28	IRF4		BATF/JUN	AICE	IL10 in Th17 responses

Yoshida 2005	16172134	HeLa	inserted	IRF4 (dominant negativ	suppression	IRF1	tandem GAAA (ISRE?)	repression of transcription TRAIL
Yamamoto Plos One 2011	22003407	macrophages		IRF4		IECS		cytokines, IL6, IL12b
Vander Lugt Nat Immunol 2014	24362890	DC (mouse)		IRF4		EICE		antigen presentation class II
Lehtonen JI 2005	16272311	MoDC, MoMF		IRF4		STAT4		DC lineage
Lehtonen JI 2005	16272311	MoDC, MoMF		IRF4		p50, p65		DC lineage
Lehtonen JI 2005	16272311	MoDC, MoMF		IRF4		PU.1		IRF4
Williams Nature Com 2014	24356538	BMDC (mouse)		IRF4		PU.1		IL10, IL33, Th2
Williams Nature Com 2014	24356538	BMDC (mouse)		IRF4				Th1 - no effect
Tussiwand Nature 2012	22992524	BMDC (mouse)		IRF4		BATF, 2,3	AICE	CD8a DC differentiation
Sciammas Immunity 2006	16919487	B cells		IRF4 high	induction	PMDR1		PMDR1, antagonising plasma cell differentation
Ochiai Immunity 2013	23684984	B cells		IRF4 high/sustained	dimerisation, low affinit	IRF4	ISRE	antagonising plasma cell differentation
Ochiai Immunity 2013	23684984	B cells		IRF4 high/sustained	dimerisation, low affinit	IRF4		PMDR1
Ochiai Immunity 2013	23684984	B cells		IRF4 low/transient		PU.1	EICE	
Ochiai Immunity 2013	23684984	B cells		IRF4 low/transient		BATF	AICE	
Ochiai Immunity 2013	23684984	B cells		IRF4 low/transient			EICE/AICE	plasma cell differentiation
Meraro JI 2002	12055236	immune cells		IRF4		PU.1	EIRE	ISRE-dependent genes
Ochiai Immunity 2013	23684984	B cells		IRF4 low/transient		PU.1		PMDR1
Rosenbauer Blood 1999	10590072			IRF4			ISRE	inhibitory
interaction				IRF4	cooperation	PU.1 (ETS)	EICE (=IECS??)	Th2
interaction				IRF4	cooperation	BATF (AP1)	AICE	Th17
interaction				IRF4	cooperation	PU.1 (ETS)	EICE (=IECS??)	CD4 Tcells/Class II presentation
interaction				IRF4 high	inhibition	IRF1	ISRE	inhibition of IRF1
Marecki JI 2001	11359842	fibroblasts (transf)		IRF8		PU.1	ISRE?? Surely EICE	IL1B
Tamura Blood 2005	15947094	macrophages (mouse)		IRF8				endocytosis and lysosyme
Huang JBC 2007	17200120	U937		IRF8		PU.1		NF1 (cytokine induced proliferation of myeloid cells)
Huang JBC 2007	17200120	U937		IRF8		IRF2/PU.1		NF1 (cytokine induced proliferation of myeloid cells)
Bovolenta PNAS 1994	8197182	Jurkat		IRF8		IRF1	ISRE	
Bovolenta PNAS 1994	8197182	Jurkat		IRF8		IRF2	ISRE	
Bovolenta PNAS 1994	8197182	Jurkat		IRF8			ISRE	inhibits binding of IRF9
Yamamoto Plos One 2011	22003407	macrophages		IRF8				cytokines, IL6, IL12b
Liu JBC 2004	15489234	macrophages (mouse)		IRF8		IRF1	*ISRE?*	IL18
Kim JI 1999	10438937	macrophage line (mouse)	LPS	IRF8		PU.1	*EICE*	IL18
Eklund JBC 1998	9593745			IRF8	PU.1 essential for the co	IRF1		CYBB = gp91 phox
Eklund JI 1999	10570299	cell lines - reporter assays	IFNg	IRF8	PU.1 essential for the co	IRF1		CYBB = gp91 phox, NCF2 = gp67 phox
Tamura Immunity 2000	10981959	Tot2 progenitor, mice		IRF8			ISRE	macrophage lineage
Tamura Immunity 2000	10981959	Tot2 progenitor, mice		IRF8		PU.1	EICE	macrophage lineage
Masumi FEBS 2002	12417340	macrophages (murine line)	IFNg priming for LPS	IRF8		IRF1	ISRE-like	IL12p40
Masumi FEBS 2002	12417340	macrophages (murine line)	IFNg priming for LPS	IRF8		IRF1	ETS/NFkB no effect	IL12p40

Tussiwand Nature 2012	22992524	BMDC (mouse)		IRF8		BATF, 2,3	AICE	CD8 T cell responses
Meraro JI 2002	12055236	immune cells		IRF8		PU.1	EIRE	ISRE-dependent genes
Smith MA JBC 2011	21216962	MoDCs, DC (mouse), THP1	LPS	IRF8/IRF4	PU.1	EICE		CIITA leading to PRDM1
Rosenbauer Blood 1999	10590072	macrophages		IRF8			ISRE	inhibitory
Weish 1994	7526889			IRF8	competition	IRF1	ISRE	MHC class I
Brass 1996	8824592	B cells		IRF4				represses IFN-inducible proliferation
Nelson 1993	7678054	N-Tera2.		IRF8	inhibits		ISRE	Interferon-induced genes
Salem 2014	25122610	dendritic cell		IRF8				dendritic cell function, CD4 and CD8 T cell activation
interaction				IRF8	cooperation	PU.1 (ETS)	EICE	CD4/Th1
interaction				IRF8	cooperation	BATF (AP-1))	AICE	CD8 T cell responses
interaction				IRF8	cooperation	IRF1	ISRE	Th1
Smith MA JBC 2011	21216962	MoDCs, DC (mouse), THP2	LPS	p65, SP1		SP1 and NFKB binding		CIITA leading to PRDM1
Weiss JI 2012	22896628	BMDC (mouse)	Lactobacillus	phagosomal processing, PI3K and MyD88		IRF1, IRF3/7		IFNb
Sciammas Immunity 2006	16919487	B cells		PMDR1	induction	IRF4 low		AICDA, plasma cell differentiation
Smith MA JBC 2011	21216962	MoDCs, DC (mouse), THP3	LPS	PRDM1	competition	IRF8	EICE	CIITA silencing
Crotty Nat Immunol 2010	20084069	B cells, T cells		PRDM1		BCL6		antagonistic interactions
Gyori Nat Immunol 2010	14985713	B Cells		PRDM1				histone lysine 9 dimethyltransferase G9a
Kuo and Calame JI 2004	15494505	B cells		PRDM1	competition	IRF1	GAAAG	IFNb
Yu 1999	10713181	B cells		PRDM1		Histone deacetylase		repression of transcription
Su 2008	19124609	B cells		PRDM1		Histone deacetylase		repression of transcription
Piskurich Nat Immunol 2000	11101876	B cells		PRDM1		CIITA		antagonistic interactions
interaction				PRDM1	competition	IRF4/8	EICE	repression of CIITA
interaction				PRDM1 induced by high	competition	IRF1	ISRE????	negative feedback loop?
Chang Immunity 2005	15963784	T cell (mouse)		PU.1				Th2 - low cytokines
Ahyi JI 2009	19592658	T cell (mouse)		PU.1		GATA3		Th2 - high cytokines
Walsh Immunity 2002	12433372	hematopoietic progenitors		PU.1		Gata-2		negative regulation of macrophage/mast cell differentiation
Smith MA JBC 2011	21216962	MoDCs, DC (mouse), THP3	LPS	PU.1		PU.1 binding		CIITA leading to PRDM1
Suzuki PNAS 1998	9600921	T cells, Mo, B cells		PU.1				gp91 phox
Ma JBC 1997	9099678	nucleic acid level	IFNg priming for LPS	PU.1			ETS2 - site, complex F3	IL12p40
Heidari Gene 2012	22659071	Neuronal cell lines					IRF/ETS binding site	Caveolin
Du PNAS 1994	7972056			NFkB		ATF-2 or cJUN/ATF	PRD2, PRD4	IFN-b
Du Cell 1993	8374955			NFkB		ATF-2 or cJUN/ATF	PRD2, PRD4	IFN-b
Cheng Science Signalling 2011	21343618	BMDM macrophages	IFNb and LPS	p50	repression	IRF3/IRF9	G-IRE, guanine rich IRE	early response, Tap1, IL15
Casola J Virol 2001	11413310	RSV infected alveoral epithelial cells		C/EBP	NF-kB	IRF,CREB/AP-1		CCL5 - multiple cis-regulation required
Heinz Mol Cell 2010	20513432	macrophages		C/EBP	CCAAT enhancer binding	PU.1	CCAAT	lineage determination
Heinz Mol Cell 2010	20513432	macrophages		C/EBP and AP1		PU.1		lineage determination
Eklund JI 1999	10570299	cell lines - reporter assays	IFNg	CBP (CREB binding protein)		IRF8/PU.1/IRF1		CYBB = gp91 phox, NCF2 = gp67 phox
Skalnik JBC 1991	1885602			CUX1	CCAAT displacement protein (repressive)		CCAAT	gp91 phox
Luo Skalnik JBC 1996	8798551			CUX1 absent		IRF2		gp91 phox
Ma JBC 1997	9099678	nucleic acid level	IFNg priming for LPS	ETS2		IRF1	ETS2 - site, complex F1	IL12p40
Ma JBC 1997	9099678	nucleic acid level	IFNg priming for LPS	ETS2			ETS2 - site, complex F2	IL12p40
Ma JBC 1997	9099678	nucleic acid level	IFNg priming for LPS	ETS2	?PU.1 - induced by IFNg	IRF1	ETS2 - site	IL12p40
interaction				TF		diverse TP		transcription partners from the same family can replace each other in the interaction

Table S3. Boolean gates

Interaction partner 1	GATE	Interaction partner 2	interaction	binding site	outcome	GATE
IRF1	and	IRF1	induction	ISRE	TH1/CD8	
IRF1	inhibition	IRF4	inhibition	ISRE	TH1/CD8	
IRF1	and	IRF8	induction	ISRE	TH1/CD8	
IRF1	not reported	AP1				
IRF1	not reported	ETS				
IRF4	and	IRF4	inhibition	ISRE	TH1/CD8	
IRF8	and	IRF8	inhibition	ISRE	TH1/CD8	OR
IRF4	and	AP1	induction	AICE	TH17	
IRF4	and	ETS	induction	EICE	TH2	OR
IRF8	and	ETS	induction	EICE	CD4	
IRF8	and	AP1	induction	AICE	CD8	OR
PRDM1	inhibition	IRF4		EICE	CD4	
PRDM1	inhibition	IRF8		EICE	CD4	OR

Table S4. Genes regulated by IRF1,4 and 8: ChIP-seq analysis

Citation	pubmed id	cell type	Stimulus	gene/ineraction	gene regulated	process
Dror Mol Immunol 2007	16597464	macrophages		IRF8	IL12p40	
Dror Mol Immunol 2007	16597464	macrophages		IRF1	IL12p40	
Dror Mol Immunol 2007	16597464	macrophages		IRF1 and IRF8	iNOS	
Dror Mol Immunol 2007	16597464	macrophages		IRF1 and IRF8	p67	
Dror Mol Immunol 2007	16597464	macrophages		IRF1 and IRF8	gp91	
Dror Mol Immunol 2007	16597464	macrophages		IRF1 and IRF8	IL-18	
Dror Mol Immunol 2007	16597464	macrophages		IRF1 and IRF8	ISG15	
Dror Mol Immunol 2007	16597464	macrophages		IRF1 and IRF8	IL-12	
Dror Mol Immunol 2007	16597464	macrophages		IRF1 and IRF8	CXCL16	Activation of Th1 immune responses
Dror Mol Immunol 2007	16597464	macrophages		IRF1 and IRF8	H28	
Dror Mol Immunol 2007	16597464	macrophages		IRF1 and IRF8	IL7R	
Dror Mol Immunol 2007	16597464	macrophages		IRF1 and IRF8	LIF	
Dror Mol Immunol 2007	16597464	macrophages		IRF1 and IRF8	MAP4K4	
Dror Mol Immunol 2007	16597464	macrophages		IRF1 and IRF8	MMP9	
Dror Mol Immunol 2007	16597464	macrophages		IRF1 and IRF8	MYC	
Dror Mol Immunol 2007	16597464	macrophages		IRF1 and IRF8	PCDH7	
Dror Mol Immunol 2007	16597464	macrophages		IRF1 and IRF8	PML	
Dror Mol Immunol 2007	16597464	macrophages		IRF1 and IRF8	SOCS7	
O'Reily JBC 2003	12676954	macrophages		PU.1	CD68	
O'Reily JBC 2003	12676954	macrophages		Fli1	CD68	
O'Reily JBC 2003	12676954	macrophages		ELF1	CD68	
O'Reily JBC 2003	12676954	macrophages		MEF	CD68	
O'Reily JBC 2003	12676954	macrophages		PU.1 and IRF4	repression of CD68	
Shi Gene 2001	21803131	monocytes		IRF1	HLA-H	
Shi Gene 2001	21803131	monocytes		IRF1	ERAP1	
Shi Gene 2001	21803131	monocytes		IRF1	TAPBP	
Shi Gene 2001	21803131	monocytes		IRF1	PSME1	
Shi Gene 2001	21803131	monocytes		IRF1	ERAP2	
Shi Gene 2001	21803131	monocytes		IRF1	PSMB9	
Shi Gene 2001	21803131	monocytes		IRF1	TAP2	
Shi Gene 2001	21803131	monocytes		IRF1	TAPBPL	
Shi Gene 2001	21803131	monocytes		IRF1	B2M	
Shi Gene 2001	21803131	monocytes		IRF1	CD209	
Shi Gene 2001	21803131	monocytes		IRF1	PSMB8	Antigen presentation class I
Shi Gene 2001	21803131	monocytes		IRF1	OAS3	
Shi Gene 2001	21803131	monocytes		IRF1	APOBEC3F	
Shi Gene 2001	21803131	monocytes		IRF1	FCGR1C	
Shi Gene 2001	21803131	monocytes		IRF1	IL29	
Shi Gene 2001	21803131	monocytes		IRF1	IL18BP	
Shi Gene 2001	21803131	monocytes		IRF1	PSEN1	
Shi Gene 2001	21803131	monocytes		IRF1	GBP1	

Shi Gene 2001	21803131	monocytes		IRF1	TLR3	
Shi Gene 2001	21803131	monocytes		IRF1	IFI35	
Shi Gene 2001	21803131	monocytes		IRF1	DHX58	
Shi Gene 2001	21803131	monocytes		IRF1	TNFRSF14	
Shi Gene 2001	21803131	monocytes		IRF1	APOL1	
Shi Gene 2001	21803131	monocytes		IRF1	ETS1	
Shi Gene 2001	21803131	monocytes		IRF1	APOBEC3G	
Shi Gene 2001	21803131	monocytes		IRF1	TNFSF13B	
Shi Gene 2001	21803131	monocytes		IRF1	IL15	
Shi Gene 2001	21803131	monocytes		IRF1	BST2	
Shi Gene 2001	21803131	monocytes		IRF1	CD274	
Tamura Blood 2005	15947094	macrophages (mouse)		IRF8	Cst3	
Tamura Blood 2005	15947094	macrophages (mouse)		IRF8	Lyzs	
Tamura Blood 2005	15947094	macrophages (mouse)		IRF8	Ctsc	
Tamura Blood 2005	15947094	macrophages (mouse)		IRF8	Psap	
Tamura Blood 2005	15947094	macrophages (mouse)		IRF8	Ctsl	
Tamura Blood 2005	15947094	macrophages (mouse)		IRF8	Pde4a	
Tamura Blood 2005	15947094	macrophages (mouse)		IRF8	Rgs2	
Tamura Blood 2005	15947094	macrophages (mouse)		IRF8	Lyn	
Tamura Blood 2005	15947094	macrophages (mouse)		IRF8	Prkcd	
Tamura Blood 2005	15947094	macrophages (mouse)		IRF8	Jak2	
Gabrielle J Leukocyt Biol 2006	16966383	DC (mouse)		IRF1	CD40	
Gabrielle J Leukocyt Biol 2006	16966383	DC (mouse)		IRF1	CD80	
Gabrielle J Leukocyt Biol 2006	16966383	DC (mouse)		IRF1	CD86	
Gabrielle J Leukocyt Biol 2006	16966383	DC (mouse)		IRF1	IL12 p40	
Gabrielle J Leukocyt Biol 2006	16966383	DC (mouse)		IRF1	IL15	
Gabrielle J Leukocyt Biol 2006	16966383	DC (mouse)		IRF1	TNFa	
Gabrielle J Leukocyt Biol 2006	16966383	DC (mouse)		IRF1	IFNg	
Ahyi JI 2009	19592658	T cell (mouse)		IRF4	IL10	
Ahyi JI 2009	19592658	T cell (mouse)		IRF4	IL4	
Glasmacher Science 2012	20064451	T cells	IL21	IRF4 and BATF	IL17	activation of Th1 immune responses
Heidari J Neuroimmunol 2011	21683457	brain			CAV1	
Honma PNAS 2008	18836070	T cell (naive)	TCR	IRF4	inhibits IL4	
Honma PNAS 2008	18836070	T cell (memory)	TCR	IRF4	promotes IL4	
Li Nature 2012	22992523	T cells	IL21, CD3-CD28	IRF4/BATF/JUN	IL10	

Yoshida 2005	16172134	HeLa	inserted	IRF1	TRAIL, DCIR	
Yamamoto Plos One 2011	22003407	hematopoietic progenitors		IRF8	macrophage development	
Yamamoto Plos One 2011	22003407	hematopoietic progenitors		IRF4	macrophage differentiation	
Yamamoto Plos One 2011	22003407	hematopoietic progenitors		IRF4	cell cycle arrest	
Yamamoto Plos One 2011	22003407	macrophages		IRF4	phagocytosis	
Vander Lugt Nat Immunol 2014	24362890	DC (mouse)		IRF4	antigen presentation in class II	antigen presentation in class II
Vander Lugt Nat Immunol 2014	24362890	DC (mouse)		IRF4	ZBTB46, CIITA, RELB, H2-DMB2, CTSS	
Vander Lugt Nat Immunol 2014	24362890	DC (mouse)		IRF8	ITGAE (CD103)	
Chopin J Exp Med 2013	24249112	LC (mouse) LC-like (mouse)		PU.1	LC development	
Chopin J Exp Med 2013	24249112	LC (mouse) LC-like (mouse)		IRF4	acquired out of epidermis	
Chopin J Exp Med 2013	24249112	LC (mouse) LC-like (mouse)		IRF4	acquired out of epidermis	
Chopin J Exp Med 2013	24249112	LC (mouse) LC-like (mouse)		PU.1	LC re-population in inflammation	
Chopin J Exp Med 2013	24249112	LC (mouse) LC-like (mouse)		PU.1	RUNX3	LC development
Chopin J Exp Med 2013	24249112	LC (mouse) LC-like (mouse)		RUNX3	LC development	
Giese J Exp Med 1997	9348311	mice		IRF8	Th1	
Liu JBC 2004	15489234	macrophages (mouse)		IRF8 and IRF1	IL12p35	
Kim JI 1999	10438937	macrophage line (mouse)	LPS	IRF8 and PU.1	IL18	
Berghout Plos Pathogens 2013	23853600	brain	neuroinflammation	IRF8	Ccl4, Ccl5, Ccl7, Ccl12, Cxcl9, Cxcl10	chemotaxis
Berghout Plos Pathogens 2013	23853600	brain	neuroinflammation	IRF8	Nlrc5, Ifi205	innate
Berghout Plos Pathogens 2013	23853600	brain	neuroinflammation	IRF8	Oasl2, Mx2, Oas1g	viral infection
Berghout Plos Pathogens 2013	23853600	brain	neuroinflammation	IRF8	Ifit2, Ifit3, Isg15, Rsad2	type1 IFN
Berghout Plos Pathogens 2013	23853600	brain	neuroinflammation	IRF8	C1q, C4b, Fcerg1	antigen capture
Berghout Plos Pathogens 2013	23853600	brain	neuroinflammation	IRF8	Irgm1, Irgm2, Igtp, Gbp2, Gbp3	phagosome maturation
Berghout Plos Pathogens 2013	23853600	brain	neuroinflammation	IRF8	Tap1, Tap2	antigen processing
Berghout Plos Pathogens 2013	23853600	brain	neuroinflammation	IRF8	B2m, H2-Ab1, H2-D, H2-K, H2-L, H2-Q, H2-T22	antigen presentation
Berghout Plos Pathogens 2013	23853600	brain	neuroinflammation	IRF8	Irf1, Irf7, Irf9	early response

Berghout Plos Pathogens 2013	23853600	IRF1-/- mice		IRF1	CD8 Tcell, no effect on CD4	
Akbari JI 2014	24489086	DC (mouse), macrophages (mouse)	L.major infection	IRF4	anti-Th1	
Akbari JI 2014	24489086	DC (mouse), macrophages (mouse)	L.major infection	IRF4	anti-IL12	
Hambleton NEJM 2011	21524210	human IRF-/-	CG infection, immune deficien	IRF8	IL12, partially IFNg, TNFa, IL10	
Hambleton NEJM 2011	21524210	human IRF-/-	CG infection, immune deficien	IRF8	DC differentiation	
Hambleton NEJM 2011	21524210	human IRF-/-	CG infection, immune deficien	IRF8	LC NOT AFFECTED	
Kamijo Science 1994	7510419	macrophages (mouse)		IRF1	NO synthesis	
Marquis Plos Genetics 2011	21731497	macrophages (mouse)	IFNg, CpG, Tuberculosis	IRF8	CD74	
Marquis Plos Genetics 2011	21731497	macrophages (mouse)	IFNg, CpG, Tuberculosis	IRF8	H2-D1	
Marquis Plos Genetics 2011	21731497	macrophages (mouse)	IFNg, CpG, Tuberculosis	IRF8	H2-DMa	
Marquis Plos Genetics 2011	21731497	macrophages (mouse)	IFNg, CpG, Tuberculosis	IRF8	H2-DMb1/2	
Marquis Plos Genetics 2011	21731497	macrophages (mouse)	IFNg, CpG, Tuberculosis	IRF8	H2-Ea	
Marquis Plos Genetics 2011	21731497	macrophages (mouse)	IFNg, CpG, Tuberculosis	IRF8	H2-Eb1	
Marquis Plos Genetics 2011	21731497	macrophages (mouse)	IFNg, CpG, Tuberculosis	IRF8	H2-Q8	
Marquis Plos Genetics 2011	21731497	macrophages (mouse)	IFNg, CpG, Tuberculosis	IRF8	Ltb	
Marquis Plos Genetics 2011	21731497	macrophages (mouse)	IFNg, CpG, Tuberculosis	IRF8	Tapbp1	antigen presentation
Marquis Plos Genetics 2011	21731497	macrophages (mouse)	IFNg, CpG, Tuberculosis	IRF8	Ccl6,	
Marquis Plos Genetics 2011	21731497	macrophages (mouse)	IFNg, CpG, Tuberculosis	IRF8	Cxcl9,	
Marquis Plos Genetics 2011	21731497	macrophages (mouse)	IFNg, CpG, Tuberculosis	IRF8	IL6ra,	
Marquis Plos Genetics 2011	21731497	macrophages (mouse)	IFNg, CpG, Tuberculosis	IRF8	Csfr3,	
Marquis Plos Genetics 2011	21731497	macrophages (mouse)	IFNg, CpG, Tuberculosis	IRF8	Fcgrt,	
Marquis Plos Genetics 2011	21731497	macrophages (mouse)	IFNg, CpG, Tuberculosis	IRF8	Tlr9	chemokines and receptors
Marquis Plos Genetics 2011	21731497	macrophages (mouse)	IFNg, CpG, Tuberculosis	IRF8	Gbp2,3,5,6,	
Marquis Plos Genetics 2011	21731497	macrophages (mouse)	IFNg, CpG, Tuberculosis	IRF8	Gma1,	
Marquis Plos Genetics 2011	21731497	macrophages (mouse)	IFNg, CpG, Tuberculosis	IRF8	Rgl2	anti-microbial GTPases
Marquis Plos Genetics 2011	21731497	macrophages (mouse)	IFNg, CpG, Tuberculosis	IRF8	CTSD	
Marquis Plos Genetics 2011	21731497	macrophages (mouse)	IFNg, CpG, Tuberculosis	IRF8	CTSB	
Marquis Plos Genetics 2011	21731497	macrophages (mouse)	IFNg, CpG, Tuberculosis	IRF8	CTSS	
Marquis Plos Genetics 2011	21731497	macrophages (mouse)	IFNg, CpG, Tuberculosis	IRF8	SLC15A3	
Marquis Plos Genetics 2011	21731497	macrophages (mouse)	IFNg, CpG, Tuberculosis	IRF8	CD74	endolytic pathway class II presentation
Marquis Plos Genetics 2011	21731497	macrophages (mouse)	IFNg, CpG, Tuberculosis	IRF8	Ifitm1	early response pathways in myeloid cells
Becker Blood 2012	22238324	myeloid and lymphoid progenitors		IRF8		DC lineage
Schlitzer Immunity 2012	23706669	DC (mouse, human)		IRF4	IL23	Th17
Persson Immunity 2013	23664832	DC (mouse, intestinal)		IRF4		Th17
Yan Virology 2004	15207617	MoLCs and MoDCs		IRF/ETS	Caveolin	Antigen cross-presentation
Antonios JI 2010	20525893	MoDCs	NiSO4	IRF	IL12p70	

Table S5. Genes regulated by expression programme "A" and "B" in the IRF-GRN

Gene Symbol	in silico TNFa/TSLP	expression values: microarray average max TNFa -T0/ average TSLP-T0
HLA-F	Programme "A"	1.661487945
CAV1	Programme "A"	1.445900654
CD40	Programme "A"	1.30052486
CD80	Programme "A"	1.236425487
TAPBPL	Programme "A"	1.233496426
CYBB	Programme "A"	1.181947045
HLA-A	Programme "A"	1.16959572
HLA-E	Programme "A"	1.164051773
CD86	Programme "A"	1.161503657
HLA-C	Programme "A"	1.160652509
IL15	Programme "A"	1.153998136
ERAP2	Programme "A"	1.149261298
NOS2	Programme "A"	1.116805394
PSME2	Programme "A"	1.110154397
TAP1	Programme "A"	1.08352888
ERAP2	Programme "A"	1.082775362
PSMB8	Programme "A"	1.041911729
HLA-B	Programme "A"	1.03594324
TAP2	Programme "A"	1.035112542
PSMB10	Programme "A"	1.025640822
IFNB	Programme "A"	1.019397771
TAPBP	Programme "A"	1.003928019
IL18BP	Programme "A"	1.000227808
PSME1	Programme "A"	0.966082654
TAP1	Programme "A"	0.963070421
ERAP1	Programme "A"	0.863455796
B2M	Programme "A"	0.806266221
IL18	Programme "A"	0.702631966
LYZ	Programme "B"	0.714557952

HLA-DPB1	Programme "B"	0.719979728
HLA-DQB1	Programme "B"	0.750181119
PRDM1	Programme "B"	0.791913837
CTSL1	Programme "B"	0.7944213
CTSD	Programme "B"	0.812923669
CTSB	Programme "B"	0.828107658
IL33	Programme "B"	0.879277268
CTSC	Programme "B"	0.881195132
CTSS	Programme "B"	0.910063224
CTSL2	Programme "B"	0.910461669
CIITA	Programme "B"	0.94038742
SLC15A3	Programme "B"	1.004945473
CST3	Programme "B"	1.021201608
CD74	Programme "B"	1.043747899
HLA-DMB	Programme "B"	1.047604139
HLA-DOB	Programme "B"	1.062740136
PSAP	Programme "B"	1.06518009
HLA-DRB1	Programme "B"	1.089017639
HLA-DQA1	Programme "B"	1.093025879
CTSL3	Programme "B"	1.20392131
IL10	Programme "B"	1.291658339

Table S6. Experimentally measured expression values at 0h (0-8 time block),2h (9-32 time block),8h (33-75 time block),and 24h (76-100 time block) converted to parametrisation values for each GRN entry node

	LC TNFa	LC TSLP
IRF1	0-8,325;9-32,1267;33-75,1209;76-100,1782	0-8,293;9-32,841;33-75,585;76-100,796
IRF8	0-8,89;9-32,879;33-75,200;76-100,131	0-8,63;9-32,847;33-75,203;76-100,206
IRF4	0-8,3762;9-32,4296;33-75,3067;76-100,2961	0-8,3773;9-32,4618;33-75,3638;76-100,5034
cJUN	0-8,2206;9-32,4831;33-75,3571;76-100,2797	0-8,2204;9-32,4798;33-75,3147;76-100,2207
cFOS	0-8,1072;9-32,811;33-75,153;76-100,34	0-8,1125;9-32,783;33-75,109;76-100,43
BATF	0-8,259;9-32,490;33-75,393;76-100,513	0-8,259;9-32,449;33-75,290;76-100,276
BATF3	0-8,174;9-32,299;33-75,511;76-100,697	0-8,174;9-32,270;33-75,325;76-100,469
ELF1	0-8,650;9-32,1112;33-75,724;76-100,521	0-8,669;9-32,1234;33-75,692;76-100,457
ELF4	0-8,159;9-32,244;33-75,204;76-100,198	0-8,155;9-32,238;33-75,181;76-100,163
ELK1	0-8,182;9-32,172;33-75,200;76-100,175	0-8,170;9-32,182;33-75,168;76-100,176
ELK3	0-8,194;9-32,273;33-75,249;76-100,261	0-8,272;9-32,317;33-75,248;76-100,423
ETS1	0-8,775;9-32,868;33-75,883;76-100,972	0-8,849;9-32,935;33-75,900;76-100,1292
ETS2	0-8,404;9-32,413;33-75,225;76-100,118	0-8,389;9-32,463;33-75,250;76-100,130
EHF	0-8,92;9-32,133;33-75,117;76-100,295	0-8,105;9-32,146;33-75,112;76-100,229
ELF2	0-8,234;9-32,306;33-75,209;76-100,252	0-8,241;9-32,341;33-75,231;76-100,243
ETV3	0-8,956;9-32,889;33-75,544;76-100,785	0-8,884;9-32,843;33-75,563;76-100,749
ETV6	0-8,558;9-32,412;33-75,363;76-100,392	0-8,527;9-32,489;33-75,438;76-100,448
GABPa	0-8,141;9-32,121;33-75,167;76-100,184	0-8,144;9-32,190;33-75,243;76-100,234

Table S7. Experimentally measured expression values for input nodes in LC migrating in the presence or absence of PI3K-gamma inhibitor, AS605240, average of n=2 independent donors

	medium	AS605240
IRF1	132.7546817	95.80075732
IRF8	62.16377096	49.23235916
IRF4	1100.954543	1018.206481
cJUN	337.125426	289.1024671
cFOS	39.07982017	37.31223789
BATF	18.8818089	20.11738465
BATF3	40.12633954	41.21470658
ELF1	1042.382563	1075.905004
ELF4	136.0850999	89.37748514
ELK1	123.4924816	91.81755367
ELK3	48.35778858	42.77809158
ETS1	157.9167944	127.3214019
ETS2	162.6078164	133.8398353
EHF	64.18514444	62.96805486
ELF2	53.8216346	48.73587259
ETV3	704.7474309	571.9613531
ETV6	483.8379809	437.0045973
GABPa	100.114365	103.6889617